The E3 ubiquitin ligase RNF220 maintains hindbrain *Hox* expression patterns through regulation of WDR5 stability

Huishan Wang[1,#], Xingyan Liu[2,3,#], Yamin Liu[1,4], Chencheng Yang[1,4], Yaxin Ye[1,4], Nengyin Sheng[1,5,7], Shihua Zhang[2,3,5,6,*], Bingyu Mao[1,5,*], Pengcheng Ma[1,8,*]

[1]State Key Laboratory of Genetic Resources and Evolution, Kunming Institute of Zoology, Chinese Academy of Sciences, Kunming 650223, China

[2]Academy of Mathematics and Systems Science, Chinese Academy of Science, Beijing 100190, China

[3]School of Mathematical Sciences, University of Chinese Academy of Sciences, Beijing 100049, China

[4]Kunming College of Life Science, University of Chinese Academy of Sciences, Kunming 650223, China

[5]Center for Excellence in Animal Evolution and Genetics, Chinese Academy of Sciences, Kunming 650223, China

[6]Key Laboratory of Systems Biology, Hangzhou Institute for Advanced Study, University of Chinese Academy of Sciences, Chinese Academy of Sciences, Hangzhou 310024, China

[7]Key Laboratory of Animal Models and Human Disease Mechanisms of Yunnan Province, Kunming Institute of Zoology, Chinese Academy of Sciences, Kunming, Yunnan 650223, China

[8]Lead contact

[#]Contributed equally

*Correspondence: Pengcheng Ma, kunmapch@mail.kiz.ac.cn; Bingyu Mao, mao@mail.kiz.ac.cn; or Shihua Zhang, zsh@amss.ac.cn

Abstract

The spatial and temporal linear expression of *Hox* genes establishes a regional *Hox* code, which is crucial for the anteroposterior patterning, segmentation, and neuronal circuit development of the hindbrain. RNF220, an E3 ubiquitin ligase, is widely involved in neural development via the targeting of multiple substrates. Here, we found that the expression of *Hox* genes in the pons was markedly up-regulated at the late developmental stage (post-embryonic day E15.5) in *Rnf220*$^{-/-}$ and *RnfF220*$^{+/-}$ mouse embryos. Single-nucleus RNA-seq analysis revealed different *Hox* de-repression profiles in different groups of neurons, including the pontine nuclei (PN). The *Hox* pattern was disrupted and the neural circuits were affected in the PN of *Rnf220*$^{+/-}$ mice. We showed that this phenomenon was regulated by WDR5, a key component of the TrxG complex, which can be ubiquitinated and degraded by RNF220. Intrauterine injection of WDR5 inhibitor (WDR5-IN-4) and genetic ablation of *Wdr5* in *Rnf220*$^{+/-}$ mice largely recovered the de-repressed *Hox* expression pattern in the hindbrain. In P19 embryonal carcinoma cells, the retinoic acid induced *Hox* expression was also stimulated upon *Rnf220* knockdown, which can be further rescued by *Wdr5* knockdown. In short, our data suggest a new role of RNF220/WDR5 in *Hox* pattern maintenance and pons development.

Introduction

The coordinated expression of *Hox* genes clusters is critical for axial patterning to determine the positional identities during the development of many tissues, including the hindbrain **(Frank *et al.*, 2019; Parker *et al.*, 2014; Parker *et al.*, 2020; Pöpperl *et al.*, 1993.)**. In mammals, there are 39 *Hox* genes organized in four clusters (*HoxA*-*HoxD*) and divided into 1-13 paralog groups (PG). During vertebrate development, the hindbrain forms eight metameric segmented units along the antero-posterior (A-P) axis known as rhombomeres (r), which later give rise to the cerebellum, pons and medulla later on **(Ghosh *et al.*, 2018; Parker *et al.*, 2020.)**. In the embryonic hindbrain, *Hox*1-5 are expressed in a nested overlapping fashion with rhombomere-specific boundaries. This *Hox* code is critical for rhombomeric territories establishment and cell fate determination **(Barsh *et al.*, 2017; Parker *et al.*, 2016; Parker *et al.*, 2020.)**.

At later stages, the *Hox* genes also play vital roles in neuronal migration and neural circuit formation **(Feng *et al.*, 2021; Hockman *et al.*, 2019; Kratochwil *et al.*, 2017; X. Wang *et al.*, 2013.)**. For example, the pontine nuclei (PN) in the pons acts as an information integration station between the cortex and cerebellum **(Kratochwil *et al.*, 2017; Maheshwari *et al.*, 2020.)**. The PN neurons originate at the posterior rhombic lip of r6-r8 and migrate tangentially to the rostral ventral hindbrain **(Di Meglio *et al.*, 2008; Farago *et al.*, 2006; Geisen *et al.*, 2008; Kratochwil *et al.*, 2017; Maheshwari *et al.*, 2020.)**. The PN neurons express *Hox 3-5* in a nested pattern determined by their rhombomeric origin, and maintained throughout migration and PN assembly **(Di Meglio *et al.*, 2013; Kratochwil *et al.*, 2017; Lizen *et al.*, 2017.)**. *Hox* factors are crucial for the specification, migration, cellular organization, and topographic input connectivity of PN neurons. Note that *Hox* gene expression is maintained up to postnatal and even adult stages in the hindbrain derivatives **(Farago *et al.*, 2006; Feng *et al.*, 2021; Kratochwil *et al.*, 2017.)**.

Hox pattern maintenance is generally governed by epigenetic regulators, especially the polycomb-group (PcG) and trithorax-group (trxG) complexes, which activate and repress *Hox* genes, respectively **(Bahrampour *et al.*, 2019; Chopra *et al.*, 2009; Kang *et al.*, 2022; Papp *et al.*, 2006.)**. In mammals, the COMPASS (complex of proteins associated with Set1) family of TrxG complexes act as methyltransferases. They contain different SET/MLL proteins, and a common multi-subunit core module consisting of WDR5, RbBP5, Ash2L, and DPY-30 (WRAD) **(Cenik *et al.*, 2021;**

Jambhekar *et al.*, 2019; Schuettengruber *et al.*, 2017.). WDR5 plays a central scaffolding role in these complexes and has been shown to act as a key regulator of *Hox* maintenance **(K. C. Wang *et al.*, 2011; Wysocka *et al.*, 2005.)**. It is involved in MLL-mediated *HoxA9* activation in acute myeloid leukemia (AML) and acute lymphoblastic leukemia (ALL) and is a target for drug development **(Chen *et al.*, 2021; Yu *et al.*, 2021.)**. The long noncoding RNA (lncRNA) *HOTTIP* also binds to WDR5 and recruits the MLL complex to stimulate *HoxA9* and *HoxA13* expression in prostate cancer and hepatocellular carcinoma **(Fu *et al.*, 2017; Malek *et al.*, 2017; Quagliata *et al.*, 2014; Wong *et al.*, 2020.)**.

RNF220 is an E3 ubiquitin ligase widely involved in neural development through targeting a range of proteins **(Kim *et al.*, 2018; Kong *et al.*, 2010; Pengcheng Ma & Mao, 2021; Pengcheng Ma *et al.*, 2022; Y.-B. Wang *et al.*, 2022.)**. Previous research has shown that *Rnf220*$^{-/-}$ mice exhibit neonatal lethality and *Rnf220*$^{+/-}$ mice develop severe motor impairments; however, the mechanisms responsible for these phenotypes remain incompletely understood **(Pengcheng Ma, Li, *et al.*, 2021; Pengcheng Ma *et al.*, 2019.)**. In the present study, we observed marked up-regulation of *Hox* genes in the pons of both *Rnf220*$^{+/-}$ and *Rnf220*$^{-/-}$ mice during late embryonic development. In the PN of *Rnf220*$^{+/-}$ mice, both the *Hox* expression pattern and the projection pattern from the motor cortex to the PN were disrupted. We identified WDR5 as a direct target of RNF220 for K48-linked ubiquitination and thus degradation, a mechanism critical for *Hox* regulation by RNF220. These findings revealed a novel role for RNF220 in the regulation of *Hox* genes and pons development.

Results

Rnf220 insufficiency leads to dysregulation of *Hox* expression in late embryonic pons

Rnf20 is strongly expressed in the embryonic mouse mid/hind brain **(Pengcheng Ma *et al.*, 2019; Y.-B. Wang *et al.*, 2022.)**. Based on microarray analysis, we explored changes in expression profiles in E18.5 *Rnf220*$^{+/-}$ and *Rnf220*$^{-/-}$ mouse brain. Interestingly, several *Hox* genes were up-regulated in the mouse brain of both genotypes **(*Tables 1 and 2*)**. Considering that *Hox* expression in forebeain is to low (date not shown), we focus on hindbrain and found that this phenomenon was

observed in late embryonic stages after E15.5 but not earlier (***Figure 1-figure supplement 1***). To determine the specific brain regions exhibiting aberrant *Hox* expression, we examined the expression levels of *HoxA9* and *HoxB9,* which were among the most significantly up-regulated genes, across various brain and spinal regions (***Figure 1-figure supplement 2A-D***). Notably, both *HoxA9* and *HoxB9* were exclusively up-regulated in the brainstem (***Figure 1-figure supplement 2C and D***). The mouse brainstem comprises the midbrain, pons, and medulla (***Figure 1-figure supplement 2E***). Further validation confirmed that the dysregulation of these *Hox* genes was restricted to the pons in the *Rnf220*$^{+/-}$ mice (***Figure 1-figure supplement 2F***). RNA sequencing (RNA-seq) analysis of the pons in 2-month-old *Rnf220*$^{+/-}$ mice similarly revealed an overall increase in *Hox* expression (***Figure 1A***).

To identify the specific cell population in which *Hox* genes were up-regulated, we conducted single-nucleus RNA-seq (snRNA-seq) analysis of the pons in 2-month-old wild-type (WT) and *Rnf220*$^{+/-}$ mice. In total, 125 956 cells were resolved in the WT mice and 122 266 cells were resolved in the *Rnf220*$^{+/-}$ mice, each containing an average of approximately 700 genes per cell. Subsequent uniform manifold approximation and projection (UMAP) identified 15 cell clusters, with no significant difference observed between the WT and *Rnf220*$^{+/-}$ groups (***Figure 1B and C***). These clusters were annotated based on their uniquely and highly expressed markers (**Table 3**). Among them, 10 clusters were identified as distinct neuronal groups, in addition to astrocytes, oligodendrocytes, oligodendrocyte precursors, ependymal cells, and a group not corresponding to any known cell type (***Figure 1B***). We analyzed changes in *Hox* gene expression within each cluster and found that up-regulation of *Hox* genes was most pronounced in clusters 2, 7, and 10 (***Figure 1D***), albeit with distinct profiles. For instance, *Hox8–10* were the most up-regulated genes in cluster 2, while *Hox3–5* and *Hox1–3* were the most up-regulated genes in clusters 7 and 10, respectively (***Figure 1D***). These findings indicate that *Hox* genes were specifically de-regulated in the pons of *Rnf220*$^{+/-}$ mice during late developmental stages.

P19 embryonal carcinoma cells can be induced to differentiate and express *Hox* genes upon retinoic acid (RA) administration and have been used to study *Hox* regulation (***Figure 1-figure supplement 3A***)(**Heyden *et al.*, 2003; Kondo *et al.*, 1992; Pöpperl *et al.*, 1993.**). Here, we tested the effects of *Rnf220* knockdown on RA-induced *Hox* expression in P19 cells. Without RA treatment, *Rnf220* knockdown had no induction effect on *Hox* expression (***Figure 1-figure supplement 3B***). H

However, with RA treatment, *Rnf220* knockdown increased RA-induced expression of *HoxA1*, *B1*, *A9*, and *B9* (***Figure 1E***), suggesting a general role of *Rnf220* in *Hox* regulation.

***Rnf220* insufficiency disturbs *Hox* expression pattern and circuit formation in PN**

Due to limitations in data resolution, the precise identification of each cluster was not fully resolved. We determined that cluster 10 likely represents cells derived from rhombomeres 2–5, given their expression of endogenous anterior *Hox* genes (*Hox1–3*), while cluster 7 likely represents cells derived from rhombomeres 6–8 cells, as evidenced by their expression of *Hox3–5* (***Figure 1D***). After mapping known neuron-specific markers to the clusters, PN-specific markers, including *Nfib*, *Pax6*, and *Barhl*, were enriched in cluster 7 (***Figure 2-figure supplement 1A and B***). PN neurons serve as relay cells between the cerebral cortex and cerebellum, originating at the posterior rhombic lip and migrating tangentially to their final position in the ventral part of the pons (**Di Meglio *et al.*, 2013; Kratochwil *et al.*, 2017; Maheshwari *et al.*, 2020.**). *Hox* genes are implicated in both PN patterning and circuit formation (**Kratochwil *et al.*, 2017; Maheshwari *et al.*, 2020.**). In this study, we explored the potential effects of *Rnf220* insufficiency on PN patterning. The PN were first dissected to analyze the expression of *Hox* genes (*Hox4* and *Hox5*) in both WT and *Rnf220*$^{+/-}$ mice (***Figure 2-figure supplement 1C***). The data indicated an up-regulation in *Hox4–5* expression levels in the *Rnf220*$^{+/-}$ PN (***Figure 2-figure supplement 1C***). In the PN, endogenous *Hox3–5* genes exhibit a nested expression pattern along the rostral-caudal axis, with *Hox3* ubiquitously expressed throughout the PN, *Hox4* localized to the middle and posterior regions, and *Hox5* confined to the posterior segment (**Kratochwil *et al.*, 2017.**). To ascertain whether this established pattern was disrupted in the *Rnf220*$^{+/-}$ PN, we dissected the PN of both WT and *Rnf220*$^{+/-}$ mice into rostral, middle, and caudal segments using a vibratome. Subsequent analysis of *Hox3–5* expression revealed an up-regulation in *Rnf220*$^{+/-}$ PN, with uniform detection along the rostral-caudal axis (***Figure 2A***).

PN are predominantly innervated by the cerebral cortex and *Hox* expression is critical for the formation of proper projection patterns (**Kratochwil *et al.*, 2017; Maheshwari *et al.*, 2020.**). Considering the motor deficits of *Rnf220*$^{+/-}$ mice (**Pengcheng Ma, Li, *et al.*, 2021; Pengcheng Ma *et al.*, 2019.**), we next tested

whether projection patterns were affected by anterograde tracing. A non-transneuronal tracing virus, rAAV-hSyn-EGFP-WPRE-hGH-poly A, was injected into the motor cortex of 2-month-old WT and *Rnf220*$^{+/-}$ mice to label axons sent from the motor cortex (***Figure 2B***). Green fluorescence intensity in the PN was measured after 3 weeks. In the PN, the projection range from the motor cortex was smaller in *Rnf220*$^{+/-}$ mice (***Figure 2C and D***). In addition, the projection pattern was shifted so that more fluorescence intensity was observed in the middle section in the *Rnf220*$^{+/-}$ PN compared to the wild type (***Figure 2C and D***).

Thus, *Rnf220* insufficiency disturbed both the expression level and pattern of *Hox* genes in PN and affected the projection pattern from the motor cortex.

WDR5 is an RNF220 target for K48-linked ubiquitination and degradation

As *Hox* up-regulation was observed only in the late stage of embryonic development, we reasoned that *Rnf220* may be involved in the maintenance of *Hox* expression. The *Hox* expression pattern is maintained epigenetically by the PcG and trxG complexes, which regulate the silencing and activation of *Hox* genes, respectively (**Bahrampour *et al.*, 2019; Chopra *et al.*, 2009; Kang *et al.*, 2022; Papp *et al.*, 2006.**). Indeed, we did observe local epigenetic modification changes in each *Hox* cluster in hindbrain of *Rnf220*$^{+/-}$ mice by ChIP-qPCR assays (***Figure 3-figure supplement 1A and B***). Therefore, we tested the expression of core components of PRC1/2 in the hindbrain (E18.5) and pons (2 months old) of *Rnf220*$^{+/-}$mice and found no obvious change in protein levels (***Figure 3-figure supplement 2A and B***). However, when WDR5, a key component of the trxG complex, was tested, a clear increase was observed in the hindbrain of both *Rnf220*$^{+/-}$*and Rnf220*$^{-/-}$ mouse embryos at E18.5 (***Figure 3A***), which was already evident at E16.5 (***Figure 3B***). We next tested the expression of WDR5 in the pons, cortex, and cerebellum of 2-month-old WT and *Rnf220*$^{+/-}$ mice. WDR5 was up-regulated in the pons but not in the cortex or cerebellum (***Figure 3C, Figure 3-figure supplement 2C and D***), consistent with the pons-specific *Hox* up-regulation. In addition, WDR5 also increased in the PN of *Rnf220*$^{+/-}$ mice (***Figure 3D***) and RA-treated P19 cells following *Rnf220* knockdown (***Figure 3E***). Thus, the stabilization of WDR5 was correlated with *Rnf220*-regulated *Hox* expression.

We speculated that WDR5 might be a direct target of RNF220 for ubiquitination and degradation. Indeed, WDR5 efficiently pulled down endogenous RNF220 in mouse brain stem lysate (***Figure 4A***), and RNF220 and WDR5 pulled down each

other when co-expressed in HEK293 cells (***Figure 4B and C***). Furthermore, co-expression of wild-type RNF220 but not the ligase-dead mutant (W539A) or the RING domain deletion (△Ring) form clearly reduced the expression level of WDR5 in HEK293 cells (***Figure 4D***), which was blocked by MG132, a proteasome inhibitor (***Figure 4E***). In ubiquitination assays, WDR5 ubiquitination was reduced in the lysate of the pons of *Rnf220*$^{+/-}$ mice (***Figure 4F***). Accordingly, the level of ubiquitinated WDR5 clearly increased when co-expressed with RNF220 but not the △Ring form in HEK293 cells (***Figure 4G***).

We tested whether the polyubiquitination of WDR5 by RNF220 was K48 linked, which is the major form of ubiquitination modification leading to proteasomal degradation (**Grice *et al.*, 2016.**). Indeed, the K48 ubiquitin mutant (in which all the lysines are substituted by arginines except lysine 48) was efficiently incorporated into the ubiquitinated WDR5 induced by RNF220, but not the K48R mutant (in which lysine 48 was substituted by an arginine), confirming that the polyubiquitination chains are K48-linked (***Figure 4H***). To determine the exact lysines ubiquitinated by RNF220, we tested the effects of RNF220 on the stability of different WDR5 truncates and found that the truncate remaining 1-127aa was enough to be degraded by RNF220 (***Figure 4-figure supplement 1A***). We then mutated the conserved lysines in this region to arginine individually, and found that mutation of K109, K112, or K120 reduced the ubiquitination level of WDR5 by RNF220 (***Figure 4-figure supplement 1B***). Simultaneous substitution of these three lysines with arginine (3M) greatly reduced WDR5 ubiquitination by RNF220 (***Figure 4I***). In conclusion, these findings indicate that RNF220 mediates K48-linked polyubiquitination of WDR5 primarily at residues K109, K112, and K120.

WDR5 is required for *Hox* regulation by RNF220

To investigate the requirement of WDR5 in RNF220-mediated *Hox* regulation, we first examined whether *WDR5* knockdown could mitigate the impact of *Rnf220* knockdown on *Hox* expression in RA-induced P19 cells. When P19 cells were transfected with *siWdr5* together with *siRnf220* and accompanied by RA treatment, the stimulation of *Hox* genes by *RNF220* knockdown was significantly reduced (***Figure 5A-D***). Note that the expression of *Hox* genes had no clear change upon *Wdr5* knockdown alone with or without RA treatment in P19 cells (***Figure 5-figure supplement 1***).

We also tested in mice. we first examined the potential for WDR5-IN-4, an established WDR5 inhibitor **(Aho *et al.*, 2019.)**, to rescue *Hox* up-regulation in *Rnf220*$^{+/-}$ embryos. Using *in-utero* microinjection, we injected WDR5-IN-4 or DMSO in mice at E15.5 and harvested the embryos at E18.5, with the hindbrains processed for qRT-PCR analysis (***Figure 6A***). Results showed that WDR5-IN-4 had no effect on *RNF220* expression (***Figure 6B***). Interestingly, the up-regulation of *HoxA9* and *HoxB9* in *Rnf220*$^{+/-}$ mice was reversed in the WDR5-IN-4 injected embryos (***Figure 6B***).

As loss of RNF220 stabilizes WDR5, we next tested whether WDR5 insufficiency would rescue the *Hox* expression pattern in *Rnf220*$^{+/-}$;*Wdr5*$^{+/-}$ double heterozygous embryos. *Rnf20*$^{fl/wt}$;*Nestin-Cre* mice were mated with *Wdr5*$^{fl/wt}$ mice to obtain embryos with different genotypes. The expression of *Hox* genes in the pons at P15 were analyzed by RT-PCR (***Figure 6C, Figure 6-figure supplement 1***). Results showed that the up-regulation of *Hox* in *Rnf20*$^{fl/wt}$*;Nestin-Cre* mice were markedly recovered in the *Rnf220*$^{fl/wt}$;*Wdr5*$^{fl/wt}$;*Nestin-Cre* mice (***Figure 6C, Figure 6-figure supplement 1***).

Taken together, the above findings support the involvement of WDR5 in RNF220 insufficiency-induced *Hox* up-regulation.

Discussion

During early embryonic development, the *Hox* genes are collinearly expressed in the hindbrain and spinal cord along the A-P axis to guide regional neuronal identity. Later on, the segmental *Hox* gene expression pattern in the hindbrain is maintained till at least early postnatal stages. The *Hox* genes are also expressed in adult hindbrains with restricted anterior boundaries. In addition to their early roles in progenitor cell specification, cell survival, neuronal migration, axon guidance, and dendrite morphogenesis **(Smith *et al.*, 2024.)**, *Hox* genes also play key roles in the regulation of synapse formation, neuronal terminal identity and neural circuit assembly at late stages **(Feng *et al.*, 2020; Feng *et al.*, 2021; Philippidou *et al.*, 2013.)**. However, the mechanisms and functions of *Hox* expression during late hindbrain development remain poorly established. Our work revealed a dose-dependent role of RNF220/WDR5 in the maintenance of *Hox* expression in late hindbrain development which might have a functional role in the neural circuit organization of the pons.

In mammals, the COMPASS family of histone-lysine methyltransferase

complexes is required for the maintenance of active chromatin states and thus *Hox* expression patterns **(Bahrampour *et al.*, 2019; Chopra *et al.*, 2009; Kang *et al.*, 2022; Papp *et al.*, 2006.)**. As a key component of the COMPASS-related complexes, WDR5 is involved in the developmental regulation of *Hox* genes **(Wysocka *et al.*, 2005.)**. WDR5 is required for MLL-fusion protein (MLL-FP)-induced *Hox* activation in AML and ALL **(Chen *et al.*, 2021; Yu *et al.*, 2021.)**. The lncRNA *HOTTIP* has been shown to interact with WDR5 and recruit WDR5-MLL complexes to *HoxA* to induce H3K4 trimethylation and gene activation **(Fu *et al.*, 2017; Malek *et al.*, 2017; Quagliata *et al.*, 2014; Wong *et al.*, 2020.)**. Our findings suggest that increased WDR5 levels in the hindbrain were associated with aberrant *Hox* expression at the late developmental stages. This dysregulation could be ameliorated either by WDR5 inhibition or haploinsufficiency. The observed up-regulation of *Hox* genes occurred at the epigenetic level within the *Hox* cluster, as evidenced by qRT-PCR analysis and a generalized increase in active H3K4 methylation markers. Furthermore, the stabilization of WDR5 and stimulation of *Hox* expression upon *RNF220* knockdown were also recapitulated in RA-treated P19 cells.

Interestingly, single-cell analysis revealed distinct profiles of *Hox* gene activation across different neuronal groups. Specifically, *Hox1–3* was up-regulated in cluster 10, *Hox3–5* was up-regulated in cluster 7, and *Hox7–10* was up-regulated in cluster 2. Clusters 10 and 7 naturally expressed *Hox1–3* and *Hox3–5*, respectively, suggesting that the observed *Hox* gene stimulation in these clusters could be attributed to elevated WDR5 levels induced by RNF220 insufficiency. Cluster 2 warrants particular attention, as it exhibited up-regulation of *Hox7–10* genes, which were not expressed in the WT hindbrain. This cluster was characterized as glycinergic neurons expressing Slc6a5. The functional implications of this distinct cell group and the phenotypic consequences of *Hox* gene dysregulation require further investigation. The dysregulation of *Hox* genes could have extensive implications for the development of various nuclei within the pons, affecting aspects such as cell differentiation and the formation of neural circuits. For the PN, we showed that both their structural patterning and patterns of projections originating from the motor cortex were altered in *Rnf220*$^{+/-}$ mice. Therefore, we can fully suspect that the motor impairments of *Rnf220*$^{+/-}$ mice is caused by abnormal projection of the central nervous system, and of course, more convincing experimental verification are needed.

In summary, our data support WDR5 as an RNF220 target involved in the maintenance of *Hox* expression and, consequently, the development of the pons.

Materials and Methods

Mouse strains and genotyping

All procedures involving mice were conducted in accordance with the guidelines of the Animal Care and Use Committee of the Kunming Institute of Zoology, Chinese Academy of Sciences (IACUC-PA-2021-07-018). Mice were housed under standard conditions at a temperature range of 20–22 °C, humidity of 30%–45%, and 12-h light/dark cycle. All mice used were maintained on a C57BL/6 background. *Vasa-Cre* mice were used to mate with *Rnf220* floxed mice *(Rnf220*$^{fl/fl}$) to generate *Rnf220* germ cell knockout (*Rnf220*$^{-/-}$) or heterozygote (*Rnf220*$^{+/-}$) mice. *Nestin-Cre* mice were used to mate with *Rnf220*$^{fl/fl}$ and *Wdr5* floxed mice (*Wdr5*$^{fl/fl}$) to generate conditional neural specific knockout or heterozygote mice. *Rnf220*$^{fl/wt}$;*Wdr5*$^{fl/wt}$;*Nestin-Cre* mice were obtained by crossing *Rnf220*$^{fl/wt}$;*Nestin-Cre* with *Wdr5*$^{fl/wt}$ mice.

Genotypes were determined by PCR using genome DNA from tail tips as templates. PCR primers were listed as follows: 5’-CTG TTG ATG AAG GTC CTG GTT-3’ and 5’-CAG GAA AAT CAA TAG ACA ACT T-3’ were used to detect *Rnf220* floxP carrying. 5’-CTG TTG ATG AAG GTC CTG GTT-3’ and 5’-CTG ATT TCC AGC AAC CTA AA-3’ were used to detect *Rnf220* knockout. 5’-GCC TGC ATT ACC GGT CGA TGC-3’ and 5’-CAG GGT GTT ATA AGC AAT CCC-3’ were used for *Cre* positive detection. 5’-GAA TAA CTA CTT TCC CTC AGA CC-3’ and 5’-CAG GCC AAG TAA CAG GAG GTA G-3’ were used to detect *Wdr5* floxP carrying. 5’-GAA TAA CTA CTT TCC CTC AGA CC-3’ and 5’-AGA CCC TGA GTG AGG ATA CAT AA-3’ were used to detect *Wdr5* knockout.

Cell culture

HEK293 and P19 cell lines were grown in Dulbecco’s Modified Eagle Medium (DMEM) (Gibco, C11995500BT) supplementary with 10% fetal bovine serum (FBS) (Biological Industries, 04-001-1A), 100 units/mL penicillin and 100 mg/ml streptomycin (Biological Industries, 03-031-1B). Cell cultures were maintained at 37°C in a humidified incubator with 5% CO_2. 0.5μM RA (Sigma, R2625) was used to induce *Hox* expression in P19 cells.

To achieve gene overexpression or knockdown, HEK293 and P19 cells were

transfected by Lipo2000 (Invitrogen, 11668500) according to the manufacturer's instructions. The following small interfering RNAs (siRNAs) (RiboBio) were used for *Rnf220* or *Wdr5* knockdown in P19 cells: siG2010160325456075, siG2010160325457167, or siG2010160325458259; and siWdr5: siB09924171210, siG131113135429, or siG131113135419.

Total RNA isolation and qRT–PCR

Tissue and cells were homogenized with 1 mL TRIZOL (TIANGEN, DP424), after which 200 μL of chloroform was added to the lysates for phase separation. After centrifugation at 12 000 *g* for 15 min at 4 °C, the aqueous phase (500 μL) was transferred to a new tube and mixed with equal volumes of isopropanol for RNA precipitation. After 30 min, RNA pellets were harvested by centrifugation at 12 000 *g* for 15 min at 4 °C, twice washed with 75% ethanol, and dissolved in DNase/RNase-free water.

cDNA was synthesized with Strand cDNA Synthesis Kit (ThermoScientific, K1632) according to the manufacturer's instructions. All reactions were performed at least triplicates with Light Cycler 480 SYBR Green I Master (Roche, 04707516001). Primers used for real-time polymerase chain reaction list in Table 4.

ChIP-qPCR

Fresh mouse PN tissues were fully grinded, cross-linked with 1% formaldehyde for 25 min, and stopped with addition of glycine. After gentle centrifuging, samples were collected and lysed with ChIP lysis buffer (150 mM NaCl, 25 mM Tris, pH 7.5, 1% Triton X-100, 0.1% SDS, 0.5% deoxycholate, and complete protease inhibitor cocktail) for 30 min on ice. Genomic DNA was sheared into 200-500 bp fragments by sonication. After centrifugation, the supernatants containing chromatin fragments were collected and immunoprecipitated with anti-IgG (2 μg, ProteinTech, B900610), anti-H3K27me3 (2 μg, Abcam, ab192985), or anti-H3K4me3 antibodies (2 μg, Abcam, ab8580) at 4℃ overnight. Then the immunoprecipitates coupled with protein A/G agarose beads (Santa Cruz, sc-2003) were washed sequentially by a low salt washing buffer, high salt washing buffer, LiCl washing buffer, and TE buffer. The immunoprecipitated chromatin fragments were eluted by 500 μL elution buffer for reversal of cross-linking at 65 °C overnight. Input or immunoprecipitated genomic DNA was purified by the QIAquick PCR Purification Kit (Qiagen, 28104) and used as a template for quantification PCR. The primers we used were listed as follows:

Genes	**Forward Primers**	**Reverse Primers**
actin	GCCAACCGTGAAAAGATGAC	GAGGCATACAGGGACAGCAC
gapdh	AGGTCGGTGTGAACGGATTTG	TGTAGACCATGTAGTTGAGGTCA
Rnf220	GTCTCAGTAGACAAGGACGTTCACA	GGGGTGGAGGTGTAGTAAGGAAG
Wdr5	CGTGACAGGCGGGAAGTGGA	CGGGTGACAAGCCGTGGAAAT
HoxA1	AGCTCTGTGAGCTGCTTGGT	AAAAGAAACCCTCCCAAAACA
HoxA2	TGCCATCAGCTATTTCCAGG	GATGAAGGAGAAGAAGGCGG
HoxA3	TCTTAACATGGAGGGAGCCA	TCTGAAGGCTACGTGTGCTG
HoxA4	ACGCTGTGCCCCAGTATAAG	ACCTTGATGGTAGGTGTGGC
HoxA5	CAGGGTCTGGTAGCGAGTGT	CTCAGCCCCAGATCTACCC
HoxA6	GTCTGGTAGCGCGTGTAGGT	CCCTGTTTACCCCTGGATG
HoxA7	CTTCTCCAGTTCCAGCGTCT	AAGCCAGTTTCCGCATCTAC
HoxA9	GTAAGGGCATCGCTTCTTCC	ACAATGCCGAGAATGAGAGC
HoxA10	TCTTTGCTGTGAGCCAGTTG	CTCCAGCCCCTTCAGAAAAC
HoxA11	CCTTTTCCAAGTCGCAATGT	AGGCTCCAGCCTACTGGAAT
HoxA13	CGGTGTCCATGTACTTGTCG	AGCGGCTACTACCCGTGC
HoxB1	GGTGAAGTTTGTGCGGAGAC	TTCGACTGGATGAAGGTCAA
HoxB2	GAACCAGACTTTGACCTGCC	GAGCTGGAGAAGGAGTTCCA
HoxB3	ATCTGTTTGGTGAGGGTGGA	CCGCACCTACCAGTACCACT
HoxB4	GACCTGCTGGCGAGTGTAG	CTGGATGCGCAAAGTTCAC
HoxB5	CTGGTAGCGAGTATAGGCGG	AGGGGCAGACTCCACAGATA
HoxB6	TAGCGTGTGTAGGTCTGGCG	AGCAGAAGTGCTCCACGC
HoxB7	CTTTCTCCAGCTCCAGGGTC	AACTTCCGGATCTACCCCTG
HoxB8	GAACTCCTTCTCCAGCTCCA	CACAGCTCTTTCCCTGGATG
HoxB9	TCCAGCGTCTGGTATTTGGT	GAAGCGAGGACAAAGAGAGG
HoxB13	TGCCCCTTGCTATAGGGAAT	ATTCTGGAAAGCAGCGTTTG
HoxC4	CTAATTCCAGGACCTGCTGC	AAAAATTCACGTTAGCACGGT
HoxC5	TTCTCGAGTTCCAGGGTCTG	ATTTACCCGTGGATGACCAA
HoxC6	CAGGGTCTGGTACCGAGAGTA	TCCAGATTTACCCCTGGATG
HoxC8	CAAGGTCTGATACCGGCTGT	ATCAGAACTCGTCTCCCAGC
HoxC9	AATCTGTCTCTGTCGGCTCC	AGTCTGGGCTCCAAAGTCAC
HoxC10	ACCTCTTCTTCCTTCCGCTC	ACTCCAGTCCAGACACCTCG
HoxC11	AAATGAAGGCTCCTACGGCG	TGTCGAAGAAGCGGTCGAAA

HoxC12	AATACGGCTTGCGCTTCTT	GACCCTGGCTCTCTGGTTTC
HoxC13	CTCACTTCGGGCTGTAGAGG	TCAGGTGTACTGCTCCAAGG
HoxD1	TCTGTCAGTTGCTTGGTGCT	TGAAAGTGAAGAGGAACGCC
HoxD3	ACCAGCTGAGCACTCGTGTA	AGAACAGCTGTGCCACTTCA
HoxD4	CTCCCTGGGCTGAGACTGT	CCCTGGGAACCACTGTTCT
HoxD8	GCCCGCGAAGTTTTACGGAT	TAAGTGGTCTGGGTCCTCGC
HoxD9	TTGTTTGGGTCAAGTTGCTG	CTCAGCTTGCAGCGATCA
HoxD10	TCTCCTGCACTTCGGGAC	GGAGCCCACTAAAGTCTCCC
HoxD11	AGTGAGGTTGAGCATCCGAG	ACACCAAGTACCAGATCCGC
HoxD12	TGCTTTGTGTAGGGTTTCCTCT	CTTCACTGCCCGACGGTA
HoxD13	TGGTGTAAGGCACCCTTTTC	CCCATTTTTGGAAATCATCC
Unc5b	CGTGACAGGCGGGAAGTGGA	CGGGTGACAAGCCGTGGAAAT
Pax6	AGACAACAACAAAGCGGACT	CTTCGCAAATGACAACTGAC
Barhl1	TACCAGAACCGCAGGACTAAAT	AGAAATAAGGCGACGGGAACAT
Nfib	AGAAGCCCGAAATCAAGCAG	CCAGTCACGGTAAGCACAAA
Neph2	ACAAGGTTCGGAAATGAAGTCG	GTTGCCATTAGGACGAGGAA

In utero microinjection

Pregnant mice were administered isoflurane for deep anesthesia. Following this, a laparotomy was performed to carefully extract the embryos, which were then placed on a sterile surgical drape. WDR5-IN-4 (100 μg, MedChemExpress, HY-111753A), containing 0.05% Malachite Green reagent for tracing, was injected into the hindbrain of E15.5 embryos using a finely-tapered borosilicate needle. To minimize the risk of spontaneous abortion, injections were spaced for the selected embryos. Following the injections, the uterus was returned to the abdominal cavity and infused with 2 mL of 37 °C, 0.9% saline solution. The peritoneum and abdominal skin were then sutured. Finally, the mice were placed on a heating pad to facilitate recovery from anesthesia.

Ubiquitination assay, immunoprecipitation and western blot analysis

In vivo ubiquitination, immunoprecipitation and Western blot assays were carried out as previously described **(Pengcheng Ma *et al.*, 2023.)**. The following primary antibodies were used for botting: anti-RNF220 (Sigma-Aldrich, HPA027578), anti-WDR5 (D9E11) (Cell Signaling Technology, 13105), anti-Ring1B (D22F2) (Cell Signaling Technology, 5694S), anti-Sin3B (AK-12) (Santa Cruz, sc-768), anti-EZH2

(ProteinTech, 21800-1-AP), anti-SUZ12 (Bethyl, A302-407A), anti-RYBP (A-1) (Santa Cruz, sc-374235), anti-CBX6 (H-1) (Santa Cruz, sc-393040), anti-CBX7 (G-3) (Santa Cruz; sc-376274), anti-CBX8 (C-3) (Santa Cruz, sc-374332), anti-PHC1 (D-10) (Santa Cruz, sc-390880), anti-α-Tubulin (ProteinTech, 66031-1-Ig), anti-FLAG (Sigma-Aldrich; F-7425), anti-myc (ProteinTech; 16286-1-AP), and anti-Ub (P4D1) (Santa Cruz, sc-2007)

snRNA-seq library preparation, sequencing, and data analysis

snRNA-seq libraries were prepared using the Split-seq platform **(Butler *et al.*, 2018; Rosenberg *et al.*, 2018.)**. Freshly harvested mouse pons tissues underwent nuclear extraction following previously described protocols **(Butler *et al.*, 2018; Rosenberg *et al.*, 2018.)**. In brief, mouse brain tissues were transferred into a 2 mL Dounce homogenizer containing 1mL homogenizing buffer (250 mM sucrose, 25 mM KCl, 5 mM $MgCl_2$, and 10 mM Tris-HCl [pH = 8.0], 1 mM DTT, RNase Inhibitor and 0.1% Triton X-100). The mixture was subjected to five strokes with a loose pestle, followed by 10 strokes with a tight pestle. The resulting homogenates were filtered through a 40-µm strainer into 5-mL Eppendorf tubes and subsequently centrifuged for 4 min at 600 *g* and 4 °C. The pellet was re-suspended and washed in 1 mL of PBS containing RNase inhibitors and 0.1% BSA. The nuclei were again filtered through a 40-µm strainer and quantified. These nuclei were partitioned into 48 wells, each of which contained a barcoded, well-specified reverse transcription primer, to enable in-nuclear reverse transcription. Subsequent second and third barcoding steps were carried out through ligation reactions. After the third round of barcoding, the nuclei were divided into 16 aliquots and lysed prior to cDNA purification. The resulting purified cDNA was subjected to template switching and qRT-PCR amplification, which was halted at the beginning of the plateau stage. Finally, the purified PCR products (600 pg) were used to generate Illumina-compatible sequencing libraries. Distinct, indexed PCR primer pairs were employed to label each library, serving as the fourth barcode.

The libraries underwent sequencing on the NextSeq system (Illumina) using 150-nucleotide kits and paired-end sequencing protocols. In this arrangement, Read 1 covered the transcript sequences and Read 2 contained the UMI and UBC barcode combinations. Initially, a six-nucleotide sequencing index, serving as the fourth barcode, was appended to the ends of Read 2. Subsequently, reads with more than one mismatching base in the third barcode were excluded from the dataset. Furthermore,

reads containing more than one low-quality base (Phred score ≤ 10) within the UMI region were also discarded. The sequencing results were aligned to exons and introns in the reference genome (Genome assembly GRCm38, https://www.ncbi.nlm.nih.gov/datasets/genome/GCF_000001635.20/) and aggregated intron and exon counts at the gene level were calculated by kallisto and bustools software as described (https://bustools.github.io/BUS_notebooks_R).

Following export of the matrix, quality control measures were performed to remove low-quality cells and potential doublets, as described previously **(Rosenberg *et al.*, 2018.)**. After filtering, a total of 125,956 and 122,266 cells for wild type and *Rnf220*$^{+/-}$ pons respectively remained for subsequent analysis. Seurat v2 **(Butler *et al.*, 2018.)** was used to identify HVGs within each group. Principal component analysis (PCA) and UMAP were performed to embed each cell from the reduced principal component space on a 2D map. Then clustering of cell populations and identification of differentially expressed genes were carried out as previously described **(Ma *et al.*, 2022.)**. We annotated the embryonic cell populations and lineages based on their DEGs (Table 3).

Mouse brain stereotactic injection and neuronal tracing

Mouse brain stereotactic injection and neuronal tracing were carried out as previously described with minor modifications **(Xu *et al.*, 2021.)**. Adult mice (2–3 months old) were used for anterograde monosynaptic neuronal tracing. The mice were first deeply anesthetized with isoflurane and placed into a stereotactic apparatus with the front teeth latched onto the anterior clamp. The mouth and nose of the mice were covered with a mask to provide isoflurane and keep them in an anesthetic state during the operation. The head was adjusted and maintained in horizontal by inserting ear bars into the ear canal. The hair of the head was shaved with an electric razor and cleaned using a cotton swab which was dipped in 75% alcohol. Cut the scalp along the midline with surgical scissors and make sure the bregma and the interaural line were exposed. The intersection between the bregma and interaural line was set to zero. The coordinates (−1.75, −4.9, −1.6) were applied for motor cortex localization. Each mouse received a single injection of 1 μL of rAAV-hSyn-EGFP-WPRE-hGH-poly A (Brainvta, PT-1990) viral fluid in the left hemisphere. After the injection, mice were bred for another 3 weeks for neuronal tracing before their brains were harvested for analysis.

Slice preparation

Mice subjected to stereotactic injection were euthanized, and whole brains were collected for the preparation of frozen sections. Following fixation in 4% paraformaldehyde (diluted in PBS) for 48 h, the brains were successively treated with 20% sucrose (diluted in PBS) for 48 h and 30% sucrose for 24 h. Brain tissues were then embedded in Optimal Cutting Temperature (OTC) compound (SAKURA, 4583) at −20 ℃ and sliced along the sagittal plane at a thickness of 40 μm.

Quantification and statistical analysis

The fluorescent and chemiluminescent intensities were quantified by Image J software (National Institute of Health). Statistical analyses were performed using GraphPad Prism software (GraphPad Software Inc., La Jolla, CA, USA). Comparisons were performed using the two-tailed Student's *t*-test. *p*-values of less than 0.05 were considered statistically significant (*), 0.01 were considered statistically significant (**) and 0.001 were considered statistically significant (***).

Acknowledgments

We are grateful to all members of the Mao and Zhang laboratories for discussion of and comments on the manuscript. We would like to thank the Core Technology Facility of Kunming Institute of Zoology (KIZ), Chinese Academy of Sciences (CAS) for providing us with service.

Additional information

Funding

Funder	Grant reference number	Author
National Key R&D Program of China	2021YFF0702700	Bingyu Mao
National Natural Science Foundation of China	32170965	Pengcheng Ma
Yunnan Fundamental Research Projects	202205AC160065 202201AW070009 202301AS070059	Pengcheng Ma
Yunnan Fundamental Research Projects	202101AU070137	Huishan Wang

The funders had no role in study design, data collection and interpretation, or the

decision to submit the work for publication.

Author contributions

Huishan Wang, Data curation, Formal analysis, Validation, Investigation, Visualization, Methodology, Writing – original draft; Xingyan Liu, Data curation, Software, Formal analysis, Visualization, Methodology; Yamin Liu, Validation, Investigation, Visualization, Methodology; Chencheng Yang, Investigation, Visualization, Methodology; Yaxin Ye, Investigation, Methodology; Nengyin Sheng, Conceptualization; Shihua zhang, Data curation, Software, Formal analysis; Bingyu Mao, Conceptualization, Resources, Formal analysis, Supervision, Funding acquisition, Visualization, Project administration, Writing – review and editing; Pengcheng Ma, Conceptualization, Resources, Formal analysis, Supervision, Funding acquisition, Visualization, Project administration, Writing – review and editing.

Author ORCIDs

Huishan Wang: https://orcid.org/0000-0001-5755-6606
Bingyu Mao: https://orcid.org/0000-0002-7993-3158
Pengcheng Ma: https://orcid.org/0000-0002-1067-8021

Additional flies

Data availability

All the snRNA-seq and RNA-seq raw data have been deposited in the GSA (https://ngdc.cncb.ac.cn/gsa/) with accession number is CRA013111.

References

Aho, E. R., Wang, J., Gogliotti, R. D., Howard, G. C., Phan, J., Acharya, P., Macdonald, J. D., Cheng, K., Lorey, S. L., Lu, B., Wenzel, S., Foshage, A. M., Alvarado, J., Wang, F., Shaw, J. G., Zhao, B., Weissmiller, A. M., Thomas, L. R., Vakoc, C. R., Hall, M. D., et al. 2019. Displacement of WDR5 from Chromatin by a WIN Site Inhibitor with Picomolar Affinity. *Cell Rep*, ***26***: 2916-2928.e2913. DOI:10.1016/j.celrep.2019.02.047, PMID: 30865883

Bahrampour, S., Jonsson, C., Thor, S. 2019. Brain expansion promoted by polycomb-mediated anterior enhancement of a neural stem cell proliferation program. *PLoS Biol*, ***17***: e3000163. DOI:10.1371/journal.pbio.3000163, PMID: 30807568

Barsh, G. R., Isabella, A. J., Moens, C. B. 2017. Vagus Motor Neuron Topographic Map Determined by Parallel Mechanisms of hox5 Expression and Time of Axon Initiation. *Curr Biol*, ***27***: 3812-3825.e3813. DOI:10.1016/j.cub.2017.11.022, PMID: 29225029

Butler, A., Hoffman, P., Smibert, P., Papalexi, E., Satija, R. 2018. Integrating single-cell transcriptomic data across different conditions, technologies, and species. *Nat Biotechnol*, ***36***: 411-420. DOI:10.1038/nbt.4096, PMID: 29608179

Cenik, B. K., Shilatifard, A. 2021. COMPASS and SWI/SNF complexes in development and disease. *Nat Rev Genet*, ***22***: 38-58. DOI:10.1038/s41576-020-0278-0, PMID: 32958894

Chen, W., Chen, X., Li, D., Zhou, J., Jiang, Z., You, Q., Guo, X. 2021. Discovery of DDO-2213 as a Potent and Orally Bioavailable Inhibitor of the WDR5-Mixed Lineage Leukemia 1 Protein-Protein Interaction for the Treatment of MLL Fusion Leukemia. *J Med Chem*, ***64***: 8221-8245. DOI:10.1021/acs.jmedchem.1c00091, PMID: 34105966

Chopra, V. S., Hong, J. W., Levine, M. 2009. Regulation of Hox gene activity by transcriptional elongation in Drosophila. *Curr Biol*, ***19***: 688-693. DOI:10.1016/j.cub.2009.02.055, PMID: 19345103

Di Meglio, T., Kratochwil, C. F., Vilain, N., Loche, A., Vitobello, A., Yonehara, K., Hrycaj, S. M., Roska, B., Peters, A. H., Eichmann, A., Wellik, D., Ducret, S., Rijli, F. M. 2013. Ezh2 orchestrates topographic migration and connectivity of mouse precerebellar neurons. *Science*, ***339***: 204-207. DOI:10.1126/science.1229326, PMID: 23307742

Di Meglio, T., Nguyen-Ba-Charvet, K. T., Tessier-Lavigne, M., Sotelo, C., Chédotal, A. 2008. Molecular mechanisms controlling midline crossing by precerebellar neurons. *J Neurosci*, ***28***: 6285-6294. DOI:10.1523/jneurosci.0078-08.2008, PMID: 18562598

Farago, A. F., Awatramani, R. B., Dymecki, S. M. 2006. Assembly of the brainstem cochlear nuclear complex is revealed by intersectional and subtractive genetic fate maps. *Neuron*, ***50***: 205-218. DOI:10.1016/j.neuron.2006.03.014, PMID: 16630833

Feng, W., Li, Y., Dao, P., Aburas, J., Islam, P., Elbaz, B., Kolarzyk, A., Brown, A. E., Kratsios, P. 2020. A terminal selector prevents a Hox transcriptional switch to safeguard motor neuron identity throughout life. *Elife*, ***9***. DOI:10.7554/eLife.50065, PMID: 31902393

Feng, W., Li, Y., Kratsios, P. 2021. Emerging Roles for Hox Proteins in the Last Steps of Neuronal Development in Worms, Flies, and Mice. *Front Neurosci*, ***15***: 801791. DOI:10.3389/fnins.2021.801791, PMID: 35185450

Frank, D., Sela-Donenfeld, D. 2019. Hindbrain induction and patterning during early vertebrate development. *Cellular and molecular life sciences : CMLS*, ***76***: 941-960. DOI:10.1007/s00018-018-2974-x, PMID: 30519881

Fu, Z., Chen, C., Zhou, Q., Wang, Y., Zhao, Y., Zhao, X., Li, W., Zheng, S., Ye, H., Wang, L., He, Z., Lin, Q., Li, Z., Chen, R. 2017. LncRNA HOTTIP modulates cancer stem cell properties in human pancreatic cancer by regulating HOXA9. *Cancer Lett*, ***410***: 68-81. DOI:10.1016/j.canlet.2017.09.019, PMID: 28947139

Geisen, M. J., Di Meglio, T., Pasqualetti, M., Ducret, S., Brunet, J. F., Chedotal, A., Rijli, F. M. 2008. Hox paralog group 2 genes control the migration of mouse pontine neurons through slit-robo signaling. *PLoS Biol*, ***6***: e142. DOI:10.1371/journal.pbio.0060142, PMID: 18547144

Ghosh, P., Sagerström, C. G. 2018. Developing roles for Hox proteins in hindbrain gene regulatory networks. *Int J Dev Biol*, ***62***: 767-774. DOI:10.1387/ijdb.180141cs, PMID: 30604846

Grice, G. L., Nathan, J. A. 2016. The recognition of ubiquitinated proteins by the proteasome. *Cellular and molecular life sciences : CMLS*, ***73***: 3497-3506. DOI:10.1007/s00018-016-2255-5, PMID: 27137187

Heyden, M. A. G. v. d., Defize, L. H. 2003. Twenty one years of P19 cells: what an embryonal carcinoma cell line taught us about cardiomyocyte differentiation. *Cardiovasc Res*, ***58***:

292-302. DOI:10.1016/s0008-6363(02)00771-x, PMID: 12757864

Hockman, D., Chong-Morrison, V., Green, S. A., Gavriouchkina, D., Candido-Ferreira, I., Ling, I. T. C., Williams, R. M., Amemiya, C. T., Smith, J. J., Bronner, M. E., Sauka-Spengler, T. 2019. A genome-wide assessment of the ancestral neural crest gene regulatory network. *Nat Commun*, ***10***: 4689. DOI:10.1038/s41467-019-12687-4, PMID: 31619682

Jambhekar, A., Dhall, A., Shi, Y. 2019. Roles and regulation of histone methylation in animal development. *Nat Rev Mol Cell Biol*, ***20***: 625-641. DOI:10.1038/s41580-019-0151-1, PMID: 31267065

Kang, H., Cabrera, J. R., Zee, B. M., Kang, H. A., Jobe, J. M., Hegarty, M. B., Barry, A. E., Glotov, A., Schwartz, Y. B., Kuroda, M. I. 2022. Variant Polycomb complexes in Drosophila consistent with ancient functional diversity. *Sci Adv*, ***8***: eadd0103. DOI:10.1126/sciadv.add0103, PMID: 36070387

Kim, J., Choi, T.-I., Park, S., Kim, M. H., Kim, C.-H., Lee, S. 2018. Rnf220cooperates withZc4h2to specify spinal progenitor domains. *Development*, ***145***. DOI:10.1242/dev.165340, PMID: 30177510

Kondo, T., Takahashi, N., Muramatsu, M. 1992. The regulation of the murine Hox-2.5 gene expression during cell differentiation. *Nucleic Acids Res*, ***20***: 5729-5735. DOI:10.1093/nar/20.21.5729, PMID: 1360646

Kong, Q., Zeng, W., Wu, J., Hu, W., Li, C., Mao, B. 2010. RNF220, an E3 ubiquitin ligase that targets Sin3B for ubiquitination. *Biochem Biophys Res Commun*, ***393***: 708-713. DOI:10.1016/j.bbrc.2010.02.066, PMID: 20170641

Kratochwil, C. F., Maheshwari, U., Rijli, F. M. 2017. The Long Journey of Pontine Nuclei Neurons: From Rhombic Lip to Cortico-Ponto-Cerebellar Circuitry. *Front Neural Circuits*, ***11***: 33. DOI:10.3389/fncir.2017.00033, PMID: 28567005

Lizen, B., Hutlet, B., Bissen, D., Sauvegarde, D., Hermant, M., Ahn, M. T., Gofflot, F. 2017. HOXA5 localization in postnatal and adult mouse brain is suggestive of regulatory roles in postmitotic neurons. *J Comp Neurol*, ***525***: 1155-1175. DOI:10.1002/cne.24123, PMID: 27650319

Ma, P., Li, Y., Wang, H., Mao, B., Luo, Z.-G. 2021. Haploinsufficiency of the TDP43 ubiquitin E3 ligase RNF220 leads to ALS-like motor neuron defects in the mouse. *Journal of Molecular Cell Biology*, ***13***: 374-382. DOI:10.1093/jmcb/mjaa072, PMID: 33386850

Ma, P., Liu, X., Xu, Z., Liu, H., Ding, X., Huang, Z., Shi, C., Liang, L., Xu, L., Li, X., Li, G., He, Y., Ding, Z., Chai, C., Wang, H., Qiu, J., Zhu, J., Wang, X., Ding, P., Zhou, S., et al. 2022. Joint profiling of gene expression and chromatin accessibility during amphioxus development at single-cell resolution. *Cell Rep*, ***39***: 110979. DOI:10.1016/j.celrep.2022.110979, PMID: 35732129

Ma, P., Mao, B. 2021. The many faces of the E3 ubiquitin ligase, RNF220, in neural development and beyond. *Development, Growth & Differentiation*, ***64***: 98-105. DOI:10.1111/dgd.12756, PMID: 34716995

Ma, P., Song, N.-N., Li, Y., Zhang, Q., Zhang, L., Zhang, L., Kong, Q., Ma, L., Yang, X., Ren, B., Li, C., Zhao, X., Li, Y., Xu, Y., Gao, X., Ding, Y.-Q., Mao, B. 2019. Fine-Tuning of Shh/Gli Signaling Gradient by Non-proteolytic Ubiquitination during Neural Patterning. *Cell Rep*, ***28***: 541-553.e544. DOI:10.1016/j.celrep.2019.06.017, PMID: 31291587

Ma, P., Yang, X., Kong, Q., Li, C., Yang, S., Li, Y., Mao, B. 2023. The Ubiquitin Ligase RNF220

Enhances Canonical Wnt Signaling through USP7-Mediated Deubiquitination of β-Catenin. *Mol Cell Biol*, ***34***: 4355-4366. DOI:10.1128/mcb.00731-14, PMID: 25266658

Ma,P., Wan, P. L., Li, Y.,He, C-H.,Song, N-N., Zhao, S., Wang, H., Ding, Y-Q., Mao, B., Sheng N. 2022. RNF220 is an E3 ubiquitin ligase for AMPA receptors to regulate synaptic transmission. *Sci Adv*, ***8***. PMID: 36179027

Maheshwari, U., Kraus, D., Vilain, N., Holwerda, S. J. B., Cankovic, V., Maiorano, N. A., Kohler, H., Satoh, D., Sigrist, M., Arber, S., Kratochwil, C. F., Di Meglio, T., Ducret, S., Rijli, F. M. 2020. Postmitotic Hoxa5 Expression Specifies Pontine Neuron Positional Identity and Input Connectivity of Cortical Afferent Subsets. *Cell Rep*, ***31***: 107767. DOI:10.1016/j.celrep.2020.107767, PMID: 32553152

Malek, R., Gajula, R. P., Williams, R. D., Nghiem, B., Simons, B. W., Nugent, K., Wang, H., Taparra, K., Lemtiri-Chlieh, G., Yoon, A. R., True, L., An, S. S., DeWeese, T. L., Ross, A. E., Schaeffer, E. M., Pienta, K. J., Hurley, P. J., Morrissey, C., Tran, P. T. 2017. TWIST1-WDR5-Hottip Regulates Hoxa9 Chromatin to Facilitate Prostate Cancer Metastasis. *Cancer Res*, ***77***: 3181-3193. DOI:10.1158/0008-5472.Can-16-2797, PMID: 28484075

Papp, B., Müller, J. 2006. Histone trimethylation and the maintenance of transcriptional ON and OFF states by trxG and PcG proteins. *Genes Dev*, ***20***: 2041-2054. DOI:10.1101/gad.388706, PMID: 16882982

Parker, H. J., Bronner, M. E., Krumlauf, R. 2014. A Hox regulatory network of hindbrain segmentation is conserved to the base of vertebrates. *Nature*, ***514***: 490-493. DOI:10.1038/nature13723, PMID: 25219855

Parker, H. J., Bronner, M. E., Krumlauf, R. 2016. The vertebrate Hox gene regulatory network for hindbrain segmentation: Evolution and diversification: Coupling of a Hox gene regulatory network to hindbrain segmentation is an ancient trait originating at the base of vertebrates. *Bioessays*, ***38***: 526-538. DOI:10.1002/bies.201600010, PMID: 27027928

Parker, H. J., Krumlauf, R. 2020. A Hox gene regulatory network for hindbrain segmentation. *Curr Top Dev Biol*, ***139***: 169-203. DOI:10.1016/bs.ctdb.2020.03.001, PMID: 32450960

Philippidou, P., Dasen, J. S. 2013. Hox genes: choreographers in neural development, architects of circuit organization. *Neuron*, ***80***: 12-34. DOI:10.1016/j.neuron.2013.09.020, PMID: 24094100

Pöpperl, H., Featherstone, M. S. 1993. Identification of a retinoic acid response element upstream of the murine Hox-4.2 gene. *Mol Cell Biol*, ***13***: 257-265. DOI:10.1128/mcb.13.1.257-265.1993, PMID: 8093325

Quagliata, L., Matter, M. S., Piscuoglio, S., Arabi, L., Ruiz, C., Procino, A., Kovac, M., Moretti, F., Makowska, Z., Boldanova, T., Andersen, J. B., Hämmerle, M., Tornillo, L., Heim, M. H., Diederichs, S., Cillo, C., Terracciano, L. M. 2014. Long noncoding RNA HOTTIP/HOXA13 expression is associated with disease progression and predicts outcome in hepatocellular carcinoma patients. *Hepatology*, ***59***: 911-923. DOI:10.1002/hep.26740, PMID: 24114970

Rosenberg, A. B., Roco, C. M., Muscat, R. A., Kuchina, A., Sample, P., Yao, Z., Graybuck, L. T., Peeler, D. J., Mukherjee, S., Chen, W., Pun, S. H., Sellers, D. L., Tasic, B., Seelig, G. 2018. Single-cell profiling of the developing mouse brain and spinal cord with split-pool barcoding. *Science*, ***360***: 176-182. DOI:10.1126/science.aam8999, PMID: 29545511

Schuettengruber, B., Bourbon, H. M., Di Croce, L., Cavalli, G. 2017. Genome Regulation by Polycomb and Trithorax: 70 Years and Counting. *Cell*, ***171***: 34-57. DOI:10.1016/j.cell.2017.08.002, PMID: 28938122

Smith, J. J., Kratsios, P. 2024. Hox gene functions in the C. elegans nervous system: From early patterning to maintenance of neuronal identity. *Semin Cell Dev Biol*, ***152-153***: 58-69. DOI:10.1016/j.semcdb.2022.11.012, PMID: 36496326

Wang, K. C., Yang, Y. W., Liu, B., Sanyal, A., Corces-Zimmerman, R., Chen, Y., Lajoie, B. R., Protacio, A., Flynn, R. A., Gupta, R. A., Wysocka, J., Lei, M., Dekker, J., Helms, J. A., Chang, H. Y. 2011. A long noncoding RNA maintains active chromatin to coordinate homeotic gene expression. *Nature*, ***472***: 120-124. DOI:10.1038/nature09819, PMID: 21423168

Wang, X., Zhou, F., Lv, S., Yi, P., Zhu, Z., Yang, Y., Feng, G., Li, W., Ou, G. 2013. Transmembrane protein MIG-13 links the Wnt signaling and Hox genes to the cell polarity in neuronal migration. *Proc Natl Acad Sci U S A*, ***110***: 11175-11180. DOI:10.1073/pnas.1301849110, PMID: 23784779

Wang, Y.-B., Song, N.-N., Zhang, L., Ma, P., Chen, J.-Y., Huang, Y., Hu, L., Mao, B., Ding, Y.-Q. 2022. Rnf220 is Implicated in the Dorsoventral Patterning of the Hindbrain Neural Tube in Mice. *Front Cell Dev Biol*, ***10***. DOI:10.3389/fcell.2022.831365, PMID: 35399523

Wong, C. H., Li, C. H., He, Q., Chan, S. L., Tong, J. H., To, K. F., Lin, L. Z., Chen, Y. 2020. Ectopic HOTTIP expression induces noncanonical transactivation pathways to promote growth and invasiveness in pancreatic ductal adenocarcinoma. *Cancer Lett*, ***477***: 1-9. DOI:10.1016/j.canlet.2020.02.038, PMID: 32120024

Wysocka, J., Swigut, T., Milne, T. A., Dou, Y., Zhang, X., Burlingame, A. L., Roeder, R. G., Brivanlou, A. H., Allis, C. D. 2005. WDR5 associates with histone H3 methylated at K4 and is essential for H3 K4 methylation and vertebrate development. *Cell*, ***121***: 859-872. DOI:10.1016/j.cell.2005.03.036, PMID: 15960974

Xu, L., Zheng, Y., Li, X., Wang, A., Huo, D., Li, Q., Wang, S., Luo, Z., Liu, Y., Xu, F., Wu, X., Wu, M., Zhou, Y. 2021. Abnormal neocortex arealization and Sotos-like syndrome-associated behavior in Setd2 mutant mice. *Sci Adv*, ***7***. DOI:10.1126/sciadv.aba1180, PMID: 33523829

Yu, X., Li, D., Kottur, J., Shen, Y., Kim, H. S., Park, K. S., Tsai, Y. H., Gong, W., Wang, J., Suzuki, K., Parker, J., Herring, L., Kaniskan, H., Cai, L., Jain, R., Liu, J., Aggarwal, A. K., Wang, G. G., Jin, J. 2021. A selective WDR5 degrader inhibits acute myeloid leukemia in patient-derived mouse models. *Sci Transl Med*, ***13***: eabj1578. DOI:10.1126/scitranslmed.abj1578, PMID: 34586829

Table1: Differently expressed genes identified using microarray between WT and *Rnf220*$^{+/-}$ mice.

ProbeName	WT_4B_NS	WT_7B_NS	HE_1B_NS	HE_2B_NS	HE_9B_NS	foldchange	GeneSymbo
A_51_P106443	3.9610484	3.8312478	3.911649	3.5465846	6.781389	0.3269886	Ttll4
A_51_P107039	5.9857764	6.293115	7.3528614	7.603712	8.187723	0.3274328	4930555G01
A_51_P145453	1.1030455	1.8843594	13.218153	13.073017	12.635066	0.0003574	Xist
A_51_P225484	3.8190854	4.0877843	2.6871324	1.7105145	2.3572092	3.146021	Epyc
A_51_P232207	8.870988	6.4653354	9.361305	9.746093	10.04952	0.3240584	Hoxb6
A_51_P232617	1.6583239	2.9412262	4.149042	3.8376906	4.293471	0.314739	Spag17
A_51_P246677	10.885349	8.35602	8.185716	7.150078	7.7772675	5.100983	Rec8
A_51_P250590	9.816977	12.201618	9.834278	9.617521	9.242044	3.6539768	Sbf2
A_51_P283044	7.210637	7.1668043	1.0895243	0.916043	1.0501599	71.924886	Kdm5d
A_51_P303160	3.7078912	2.96213	3.7240596	7.054022	3.409316	0.1996523	Arg1
A_51_P305532	9.002047	9.349363	7.1329226	7.1292458	7.182117	4.1062864	Eif2s3x
A_51_P307944	5.1118865	4.8116364	1.2979898	0.8410812	0.8931325	15.390296	S1pr4
A_51_P353232	8.54968	5.1697693	4.654748	5.1941752	5.279355	6.1218148	Tnnc2
A_51_P355122	9.005632	6.4512677	6.390123	6.4971147	6.698944	3.2444464	Tnni2
A_51_P398491	3.57301	3.2548206	0.7871613	2.121579	1.9185144	3.2634084	Trem1
A_51_P401659	8.49288	13.804942	8.294904	8.26872	8.293301	23.508588	Sspn
A_51_P402686	5.390537	0.7771567	6.5473924	7.4789324	8.404096	0.1072456	Hoxb8
A_51_P402994	7.67957	7.889223	0.889564	0.9211274	1.5682712	98.803163	Ddx3y
A_51_P413147	2.9268467	3.3636706	4.4126472	4.0533743	5.4956694	0.3233795	Klk1b3
A_51_P416858	7.626576	3.8670025	4.1174607	4.1858187	4.177822	5.9325753	Myl1
A_51_P447189	7.250779	4.738179	5.3955793	3.4247038	1.976046	4.7295439	LOC100503
A_51_P479715	8.826565	9.364602	0.9919275	0.9381926	1.0508884	279.38628	Eif2s3y
A_51_P496245	3.5971034	0.8649594	4.750976	5.8702064	8.07007	0.0589677	Hoxc6
A_51_P509263	5.1390595	4.7569666	5.2049723	6.028042	8.534603	0.1975087	Hoxa7
A_52_P106285	7.450177	5.0501213	4.8360424	4.7674747	5.396261	3.1865628	Rnf157
A_52_P113537	0.7702979	0.7451581	9.380402	9.468647	8.730086	0.0028187	Xist
A_52_P129547	2.2627034	2.8756747	4.0872307	3.994681	4.994796	0.2808802	Cdh10
A_52_P194971	7.003126	2.4153306	7.9176655	8.676689	9.467014	0.1475055	Hoxb7
A_52_P245806	2.0121722	2.2222986	8.024733	8.075076	7.757375	0.0174827	Tsix
A_52_P247537	5.6644816	5.820669	1.1234794	1.0404364	1.3392673	23.775287	
A_52_P275069	5.1697693	5.7891135	3.00036	3.540889	4.4741592	3.2708292	Gm6792
A_52_P300376	0.8213641	0.7698782	7.833779	7.7910423	7.6257606	0.0080483	Xist
A_52_P315942	2.6382132	1.1713203	3.8614466	3.9763458	3.6737823	0.2954844	Ptpn6
A_52_P320156	1.7486724	4.2580724	4.245352	5.562554	5.2181706	0.326164	E430024C06
A_52_P328825	9.731535	9.426588	11.306289	11.323352	11.139886	0.3138731	Wdfy1
A_52_P362360	0.9219009	0.8588854	11.556221	11.669298	11.221105	0.0006426	Xist
A_52_P369840	4.6016273	3.4662702	3.311216	1.8128297	0.9486678	3.4481878	2900060N12
A_52_P411296	9.834575	12.287046	9.773543	9.764503	9.759869	3.3943711	Sh3kbp1
A_52_P415996	6.9113474	5.664976	5.3968697	4.112598	4.4212303	3.1742972	Gstm6

A_52_P420563	6.4848566	12.048418	6.416327	6.674661	6.382933	23.939071	Ncor2
A_52_P424550	1.298509	0.9006791	4.036758	2.8420594	3.6169257	0.1810222	
A_52_P459732	8.02701	6.3407764	5.81404	5.444841	5.9562135	3.1675232	Rec8
A_52_P620944	3.8066573	3.6602871	1.5122881	1.4530756	0.9071637	5.3516229	
A_52_P755632	3.5135806	4.4207397	4.49904	4.160672	8.204504	0.1468263	
A_52_P763332	1.06057	5.5879946	6.3257084	7.2547207	6.8896036	0.2141694	
A_52_P909122	9.128128	12.63704	10.234246	9.10839	9.897138	3.8354481	
A_52_P940338	0.8494085	2.08987	4.3664184	2.8508143	5.45008	0.1270092	LOC382202
A_52_P980199	2.3094199	2.2522495	4.359635	4.6852355	3.6413543	0.2482597	Cdh10
A_52_P98462	0.6979232	0.7272494	2.9216394	3.5460274	7.518462	0.0242659	Hoxb9

Table2 : Differently expressed genes identified using microarray between WT and *Rnf220*$^{-/-}$ mice.

ProbeName	WT_4B_NS	WT_7B_NS	KO_3B_NS	KO_5B_NS	KO_6B_NS	foldchange	GeneSymb
A_51_P125351	6.313856	6.601757	6.4720597	6.4195724	10.480064	0.1653608	Lce1b
A_51_P132185	6.5295115	6.335476	7.368577	6.2388043	11.309154	0.0934783	Stfa1
A_51_P135944	4.8749924	4.083627	5.2269435	4.498599	9.086301	0.1150532	Stfa2
A_51_P170059	3.6045246	4.311549	3.71578	3.9532177	10.690251	0.0285741	Lce1m
A_51_P183197	4.167489	4.6221843	4.5278687	4.208487	8.697207	0.1399295	2310002J15
A_51_P214127	3.6033967	2.9677386	3.4971817	4.097985	8.025378	0.1037036	Cpa3
A_51_P232207	8.870988	6.4653354	9.991578	10.203091	9.469767	0.2872938	Hoxb6
A_51_P250590	9.816977	12.201618	9.5322485	9.307759	9.114188	4.3656323	Sbf2
A_51_P260265	6.1705537	5.226247	7.260891	7.727149	7.3651867	0.3097302	Hoxd4
A_51_P287198	4.01975	4.0344496	3.9391453	3.7721603	7.729372	0.2027683	Krt23
A_51_P296109	4.4744844	3.92833	4.659961	4.587028	7.9215555	0.1925611	Dmkn
A_51_P303784	4.194939	3.565834	1.1152956	1.1867241	2.18678	5.0285685	Olfr218
A_51_P307944	5.1118865	4.8116364	0.8316174	0.7184657	0.8546457	17.960621	S1pr4
A_51_P321011	6.994348	7.199608	3.8395464	4.032716	3.4444318	9.9049398	
A_51_P336830	4.502313	2.8254704	3.985986	3.6439693	8.376842	0.1237058	Fabp4
A_51_P336833	4.593224	3.1738102	4.121704	3.8008437	8.382238	0.1362804	Fabp4
A_51_P384894	7.477057	7.303433	8.060354	7.1584826	12.393815	0.0870583	Csta
A_51_P393968	5.735548	5.217275	2.2287815	1.0561386	1.0544479	15.346941	Vsx2
A_51_P401659	8.49288	13.804942	8.375488	8.372072	8.301443	22.48262	Sspn
A_51_P402686	5.390537	0.7771567	8.055451	8.566343	6.7811	0.0867356	Hoxb8
A_51_P444543	5.1029267	5.1083794	3.17601	2.371889	2.719416	4.9660082	Dbh
A_51_P461040	6.6832285	6.5802245	6.843542	6.9395475	10.69976	0.1566059	Crct1
A_51_P474752	3.7151783	3.267671	0.8849869	0.8739997	0.8531357	6.2244189	Ucn2
A_51_P496245	3.5971034	0.8649594	6.764801	8.603234	4.844242	0.0396761	Hoxc6
A_51_P499698	5.7629433	5.356135	5.2179017	5.541067	10.220467	0.1119105	Asprv1
A_51_P504815	5.939404	5.932974	6.521724	5.831172	12.178275	0.0384009	Stfa3
A_51_P509263	5.1390595	4.7569666	7.245264	8.561127	5.753749	0.1601265	Hoxa7
A_51_P514035	5.6431694	4.7971907	5.6459165	6.3477407	10.138423	0.0926953	Cma1
A_52_P117920	5.120014	3.3515055	3.6814542	3.3344727	8.7837105	0.1455336	
A_52_P117922	4.337855	4.06896	4.056633	3.9852946	9.184422	0.0903605	
A_52_P171692	5.2034197	4.5558033	5.1785574	4.851259	8.4255705	0.2214345	1190003J15
A_52_P194971	7.003126	2.4153306	9.013775	9.578628	8.266773	0.1260852	Hoxb7
A_52_P240842	4.914063	1.2371906	5.9930615	6.191735	5.1821957	0.2816936	9430077A0
A_52_P347956	0.7941967	0.9586504	4.051279	4.083244	3.9578302	0.1124228	Cyp2j13
A_52_P411296	9.834575	12.287046	9.918812	9.747645	9.758842	3.2910543	Sh3kbp1
A_52_P420563	6.4848566	12.048418	6.4241385	6.346026	6.5670357	24.760186	Ncor2
A_52_P436122	2.9213138	3.0083542	5.30703	5.467043	5.6950293	0.1727731	
A_52_P445239	3.697067	5.3639936	3.4139938	3.297052	2.1909828	3.2421623	Plp1

A_52_P487686	6.869822	6.442713	7.520336	6.6244674	11.930332	0.0730948	BC100530
A_52_P523368	4.5968947	4.545647	4.597747	4.583084	7.504041	0.3105278	Psapl1
A_52_P531325	5.7284603	5.8114233	1.0499647	1.0681556	2.071632	19.56396	Rps6
A_52_P620944	3.8066573	3.6602871	0.8701608	0.7867022	0.8770287	7.4133046	
A_52_P673122	3.6899672	3.9134355	2.7354527	0.9638019	2.2010896	3.1768653	
A_52_P909122	9.128128	12.63704	10.752602	9.08155	9.953282	3.1899222	
A_52_P98614	6.431283	5.7046127	1.0239266	1.010514	0.9768893	34.518845	Slc6a2

Table3: Differently expressed genes of pons identified using snRNA-seq between WT and *Rnf220*$^{+/-}$ mice.

	p_val	avg_logFC	pct.1	pct.2	cluster
Snhg11	0	0.9540666	0.993	0.814	0
Zfp101	0	0.7367873	0.832	0.746	0
Ube3a	0	0.5335392	0.613	0.483	0
D10Wsu102e	0	0.4966353	0.707	0.571	0
Srrm2	0	0.4596324	0.663	0.549	0
AC149090.1	0	0.4474371	0.441	0.301	0
Mmachc	0	0.4081537	0.411	0.296	0
Vmn2r53	0	0.375206	0.426	0.302	0
Pnisr	0	0.3638224	0.487	0.389	0
Rbm25	0	0.3391598	0.515	0.454	0
Nktr	0	0.3348808	0.401	0.305	0
Fus	0	0.3149181	0.424	0.352	0
Syne1	0	0.3130419	0.5	0.447	0
Gm17132	0	0.3126096	0.349	0.257	0
Usp19	0	0.2997827	0.335	0.265	0
Cenpc1	0	0.2940808	0.284	0.199	0
Gm48119	0	0.2927253	0.306	0.21	0
Vmn2r76	0	0.2875166	0.301	0.208	0
Gria2	0	0.2844672	0.458	0.404	0
Luc7l2	0	0.2652363	0.33	0.271	0
Dennd1b	0	0.2634844	0.282	0.212	0
Tmem72	0	0.257478	0.34	0.287	0
Epha5	0	0.2546523	0.332	0.291	0
Snrnp70	0	0.2524077	0.35	0.296	0
Nap1l5	0	0.6473373	0.758	0.393	1
Gad2	0	0.4701617	0.375	0.121	1
Scg2	0	0.4498357	0.503	0.249	1
Ahi1	0	0.4384739	0.506	0.197	1
Gprasp1	0	0.3767198	0.609	0.364	1
6330403K07Rik	0	0.3761973	0.358	0.077	1
Tmem130	0	0.3663431	0.466	0.22	1
Celf4	0	0.3487743	0.501	0.241	1
Peg3	0	0.3147951	0.775	0.588	1
Impact	0	0.3073325	0.433	0.22	1
Gap43	0	0.2998809	0.325	0.107	1
Pnmal2	0	0.297587	0.433	0.22	1
Zwint	0	0.2867501	0.526	0.333	1

Resp18	0	0.2630204	0.322	0.167	1
Nefm	0	0.7882714	0.875	0.396	2
Snap25	0	0.6622256	0.93	0.556	2
Nefh	0	0.6536582	0.736	0.249	2
Map1b	0	0.6242659	0.958	0.646	2
Atp1b1	0	0.6146502	0.954	0.669	2
Cplx1	0	0.6064388	0.795	0.319	2
Sparcl1	0	0.5704161	0.825	0.366	2
Calm1	0	0.5449357	0.902	0.611	2
Atp1a3	0	0.5418078	0.765	0.448	2
Nefl	0	0.5120509	0.704	0.297	2
Pkm	0	0.4929712	0.82	0.423	2
Vsnl1	0	0.4829055	0.733	0.305	2
Map1a	0	0.4735071	0.773	0.383	2
Lars2	0	0.4709724	0.969	0.834	2
Syt2	0	0.4691961	0.684	0.247	2
Kcnc3	0	0.4638185	0.599	0.199	2
Slc25a4	0	0.4524251	0.791	0.461	2
Kcna2	0	0.4155329	0.699	0.288	2
Vamp1	0	0.4013327	0.687	0.27	2
Lamp5	0	0.3926798	0.501	0.15	2
Slc6a5	0	0.3915305	0.373	0.108	2
Ndrg4	0	0.3745433	0.75	0.378	2
Ckb	0	0.3706504	0.725	0.374	2
Map7d2	0	0.3696816	0.65	0.294	2
Hsp90aa1	0	0.3623147	0.815	0.496	2
Stmn3	0	0.36053	0.67	0.334	2
Kcna1	0	0.3599023	0.601	0.222	2
Gm20594	0	0.3511162	0.862	0.561	2
Mdh1	0	0.3501233	0.685	0.325	2
Calm3	0	0.3483847	0.663	0.301	2
Gapdh	0	0.3429265	0.598	0.371	2
Calm2	0	0.342898	0.8	0.465	2
Ldhb	0	0.3426175	0.638	0.264	2
Ghitm	0	0.3340682	0.647	0.273	2
Ina	0	0.3311065	0.563	0.21	2
Atp5b	0	0.3296494	0.76	0.429	2
Ywhag	0	0.3289253	0.674	0.305	2
Hspa8	0	0.3254792	0.695	0.394	2
Scn1a	0	0.3190687	0.688	0.33	2
mt-Nd1	0	0.3189891	0.65	0.327	2
mt-Cytb	0	0.3017935	0.723	0.395	2
Napb	0	0.2963015	0.71	0.386	2

Nars	0	0.295612	0.617	0.287	2
Hsp90ab1	0	0.294607	0.843	0.561	2
Nat8l	0	0.2926316	0.591	0.204	2
Rtn3	0	0.2911262	0.705	0.371	2
Aldoc	0	0.2879719	0.629	0.286	2
Atp2b2	0	0.282642	0.651	0.311	2
Dnm1	0	0.2807882	0.604	0.289	2
Eno2	0	0.2807822	0.647	0.297	2
Glra1	0	0.2801859	0.558	0.213	2
Sv2c	0	0.2795559	0.472	0.151	2
Scn8a	0	0.277919	0.621	0.277	2
Rph3a	0	0.2774697	0.519	0.173	2
Atp2a2	0	0.2686874	0.642	0.309	2
Nsf	0	0.2676745	0.696	0.369	2
Slc24a2	0	0.26494	0.594	0.254	2
Atp6v1a	0	0.2648543	0.658	0.341	2
Cltc	0	0.2623385	0.617	0.293	2
mt-Nd2	0	0.252835	0.532	0.269	2
Clstn1	0	0.250687	0.632	0.3	2
Plp1	0	3.4437013	0.991	0.211	3
Trf	0	1.8707847	0.803	0.058	3
Mag	0	1.7196174	0.799	0.033	3
Apod	0	1.6560469	0.607	0.039	3
Fth1	0	1.6308212	0.792	0.436	3
Ptgds	0	1.5264231	0.343	0.098	3
Scd2	0	1.4443092	0.764	0.222	3
Mbp	0	1.4301111	0.782	0.14	3
Cnp	0	1.4203155	0.663	0.036	3
Mobp	0	1.3381085	0.696	0.087	3
Car2	0	1.2150987	0.543	0.046	3
Mal	0	1.2013232	0.523	0.02	3
Qk	0	1.1079033	0.594	0.064	3
Gpm6b	0	1.0702732	0.564	0.071	3
Aplp1	0	1.0540449	0.636	0.222	3
Ermn	0	0.987124	0.471	0.012	3
Glul	0	0.9430473	0.453	0.064	3
Slc12a2	0	0.8725496	0.479	0.075	3
Ugt8a	0	0.8402525	0.427	0.038	3
Ptprd	0	0.820107	0.602	0.295	3
Enpp2	0	0.7993549	0.648	0.088	3
S100b	0	0.7940206	0.373	0.13	3
Tubb4a	0	0.7869016	0.431	0.212	3
Mog	0	0.7455389	0.362	0.009	3

Cryab	0	0.6964547	0.316	0.018	3
Gjc3	0	0.6954245	0.353	0.023	3
Abca2	0	0.6672388	0.462	0.246	3
Cntn2	0	0.6642329	0.376	0.115	3
Cldn11	0	0.6627474	0.303	0.008	3
7-Sep	0	0.6565189	0.476	0.277	3
Zeb2	0	0.6306229	0.347	0.047	3
Stmn4	0	0.6265405	0.339	0.059	3
Map7	0	0.6238302	0.331	0.042	3
4-Sep	0	0.6116378	0.355	0.14	3
Gsn	0	0.602966	0.279	0.007	3
Ptma	0	0.5983608	0.353	0.133	3
Klk6	0	0.596435	0.236	0.003	3
Syt11	0	0.5895886	0.669	0.548	3
Fnbp1	0	0.5812498	0.383	0.168	3
Actb	0	0.5724746	0.628	0.52	3
Qdpr	0	0.5626731	0.286	0.072	3
Cmtm5	0	0.5616848	0.263	0.009	3
Kcnj10	0	0.5520853	0.288	0.024	3
Lamp1	0	0.531557	0.335	0.153	3
Hapln2	0	0.5287375	0.247	0.006	3
Pex5l	0	0.5259814	0.304	0.091	3
Ndrg1	0	0.5249046	0.256	0.012	3
Tmem88b	0	0.5231319	0.254	0.022	3
Efcab14	0	0.5167435	0.279	0.077	3
Dock9	0	0.5114567	0.318	0.137	3
Kif1b	0	0.5100938	0.607	0.504	3
Tmem151a	0	0.5016586	0.289	0.116	3
Prr5l	0	0.4861403	0.23	0.007	3
Plxnb3	0	0.4751939	0.211	0.007	3
Rtn4	0	0.4746112	0.425	0.323	3
Tspan2	0	0.4740951	0.218	0.017	3
Adamts4	0	0.4727044	0.231	0.009	3
Dock10	0	0.4721793	0.255	0.042	3
Cd81	0	0.4688141	0.309	0.174	3
Sez6l2	0	0.4638343	0.326	0.206	3
Selenop	0	0.4599166	0.215	0.018	3
Aatk	0	0.4584498	0.264	0.106	3
Hmgcs1	0	0.4515978	0.299	0.18	3
Pcdh9	0	0.4486376	0.445	0.323	3
Phldb1	0	0.4436813	0.204	0.017	3
Tuba1a	0	0.4378003	0.347	0.26	3
Tmem63a	0	0.4376406	0.207	0.005	3

Kndc1	0	0.4354788	0.289	0.165	3
Slc48a1	0	0.4345389	0.241	0.071	3
Plekhh1	0	0.4289592	0.2	0.015	3
Ywhaq	0	0.4219728	0.318	0.223	3
Edil3	0	0.4199897	0.285	0.145	3
Fgfr2	0	0.4143634	0.2	0.02	3
Otud7b	0	0.4113574	0.231	0.059	3
Efnb3	0	0.4088633	0.202	0.009	3
Anln	0	0.400709	0.194	0.015	3
Rnf13	0	0.3953748	0.238	0.088	3
Agpat4	0	0.3866612	0.207	0.036	3
Cdc37l1	0	0.3860095	0.285	0.171	3
Gjc2	0	0.3806491	0.179	0.004	3
Lpar1	0	0.3783473	0.185	0.007	3
Adipor2	0	0.3777323	0.187	0.035	3
Secisbp2l	0	0.3754237	0.212	0.06	3
Fez1	0	0.3746373	0.249	0.142	3
Myrf	0	0.3745537	0.185	0.021	3
Nfasc	0	0.371303	0.303	0.265	3
Pmp22	0	0.3701979	0.164	0.012	3
Sirt2	0	0.3635241	0.21	0.071	3
Shisa4	0	0.3625061	0.215	0.09	3
Tmeff2	0	0.3618407	0.214	0.075	3
Kif13b	0	0.3591705	0.195	0.047	3
Sec11c	0	0.3536522	0.207	0.079	3
Daam2	0	0.3526074	0.182	0.037	3
Slc44a1	0	0.3515341	0.189	0.04	3
Arhgap23	0	0.3510998	0.18	0.04	3
Itm2b	0	0.3506868	0.356	0.302	3
Cpd	0	0.3491617	0.188	0.052	3
Zdhhc20	0	0.3481961	0.257	0.161	3
Pacs2	0	0.347316	0.198	0.063	3
Wscd1	0	0.341744	0.175	0.037	3
Tppp3	0	0.336165	0.191	0.088	3
Ttyh2	0	0.3342392	0.159	0.008	3
Atp1b3	0	0.329504	0.189	0.07	3
Aspa	0	0.3264428	0.158	0.014	3
Stmn1	0	0.3257563	0.228	0.123	3
Pea15a	0	0.3252495	0.203	0.09	3
Etv1	0	0.32521	0.152	0.014	3
Plin3	0	0.3230782	0.148	0.01	3
Gjb1	0	0.3226736	0.148	0.002	3
Taldo1	0	0.322439	0.168	0.04	3

Serpinb1a	0	0.3173902	0.143	0.003	3
Arhgef10	0	0.3167752	0.151	0.013	3
Usp54	0	0.3166988	0.171	0.044	3
Dbndd2	0	0.3153281	0.172	0.05	3
Enpp4	0	0.3150774	0.162	0.035	3
Elovl1	0	0.3143994	0.15	0.009	3
Sec14l5	0	0.314212	0.147	0.014	3
Wnk1	0	0.3140146	0.257	0.188	3
Magt1	0	0.3065059	0.155	0.026	3
Npc1	0	0.3014844	0.184	0.074	3
Psat1	0	0.3003193	0.147	0.022	3
Cpox	0	0.299684	0.161	0.048	3
Slc38a2	0	0.2976823	0.226	0.164	3
Tppp	0	0.2973396	0.181	0.086	3
Ptn	0	0.2962332	0.179	0.099	3
Pik3c2b	0	0.2950909	0.164	0.047	3
Gltp	0	0.2946176	0.14	0.009	3
Kctd3	0	0.2930424	0.206	0.115	3
Cers2	0	0.2929419	0.151	0.018	3
Kctd13	0	0.2920035	0.146	0.025	3
Phlpp1	0	0.291286	0.154	0.031	3
Eef1a1	0	0.2910657	0.259	0.19	3
Mast4	0	0.2900613	0.213	0.133	3
Myo6	0	0.2893583	0.175	0.061	3
Ankrd28	0	0.2875955	0.175	0.066	3
Fa2h	0	0.2862184	0.135	0.005	3
Sort1	0	0.284055	0.194	0.121	3
Nrbp2	0	0.2810097	0.158	0.047	3
Bin1	0	0.2803092	0.254	0.219	3
Eml1	0	0.2798412	0.145	0.022	3
Ppp1r16b	0	0.2772155	0.162	0.061	3
Csrp1	0	0.2769179	0.129	0.013	3
Plekhb1	0	0.2768113	0.136	0.012	3
Olig1	0	0.2754197	0.127	0.006	3
Foxn3	0	0.2744346	0.185	0.107	3
Sccpdh	0	0.2725627	0.164	0.073	3
Dpy19l1	0	0.2709104	0.146	0.036	3
Gnao1	0	0.2688801	0.284	0.253	3
Elovl7	0	0.2688145	0.134	0.019	3
Sypl	0	0.2686733	0.147	0.034	3
Inf2	0	0.2684947	0.129	0.008	3
S100a16	0	0.2631298	0.119	0.005	3
Arrdc3	0	0.2628438	0.135	0.028	3

Tmbim1	0	0.2586548	0.157	0.054	3
Arhgef2	0	0.2572418	0.151	0.047	3
Car14	0	0.2563609	0.126	0.008	3
Josd2	0	0.2548116	0.135	0.028	3
Arsg	0	0.2546638	0.122	0.013	3
Ccp110	0	0.2527608	0.139	0.05	3
Ckb1	0	0.4836905	0.724	0.433	4
Pvalb	0	0.4661873	0.413	0.109	4
Sphkap	0	0.438224	0.399	0.08	4
Ppp3ca	0	0.4227978	0.525	0.304	4
Sparcl11	0	0.4128678	0.744	0.447	4
Necab2	0	0.3931824	0.31	0.025	4
Scn4b	0	0.3793392	0.361	0.137	4
Map1a1	0	0.3768442	0.704	0.452	4
Nefm1	0	0.3686965	0.809	0.479	4
Nefl1	0	0.3585811	0.663	0.367	4
Glra11	0	0.3544084	0.505	0.273	4
Slc17a6	0	0.3484613	0.504	0.209	4
AI593442	0	0.3483056	0.371	0.138	4
Vsnl11	0	0.343443	0.618	0.381	4
Snap251	0	0.341713	0.862	0.622	4
Atp1b11	0	0.3404215	0.922	0.718	4
Cplx11	0	0.3299008	0.644	0.405	4
Atp5b1	0	0.3276665	0.695	0.487	4
Ebf1	0	0.3085761	0.297	0.08	4
Arpp21	0	0.304836	0.389	0.139	4
Calm21	0	0.3026335	0.723	0.524	4
Ntng1	0	0.3000027	0.285	0.063	4
Sptb	0	0.2974729	0.308	0.133	4
Tanc1	0	0.2920494	0.295	0.078	4
Cplx2	0	0.2859935	0.31	0.131	4
Chgb	0	0.2855212	0.485	0.303	4
Ldhb1	0	0.2806631	0.53	0.331	4
Vamp11	0	0.2794603	0.546	0.346	4
Rgs7bp	0	0.2751283	0.381	0.198	4
Pitpnc1	0	0.2680408	0.283	0.094	4
Ina1	0	0.2599847	0.441	0.274	4
Plcb4	0	0.2589942	0.389	0.219	4
Smarca2	0	0.2534591	0.459	0.295	4
Stmn31	1.78E-266	0.2545976	0.552	0.396	4
Atp1a31	6.78E-265	0.3353992	0.668	0.505	4
Apoe	0	1.6086973	0.577	0.055	5
Atp1a2	0	1.5247581	0.674	0.031	5

Sparc	0	1.0838668	0.476	0.03	5
Slc1a2	0	1.0801745	0.466	0.047	5
Ptgds1	0	1.0527407	0.236	0.113	5
Cst3	0	0.9195035	0.414	0.152	5
Atp1b2	0	0.7810754	0.351	0.044	5
Aqp4	0	0.6686322	0.258	0.005	5
Slc4a4	0	0.6680274	0.297	0.028	5
Rgs5	0	0.6562534	0.187	0.007	5
Gm205941	0	0.6442261	0.675	0.621	5
Mbp1	0	0.6325801	0.391	0.181	5
Sparcl12	0	0.631754	0.618	0.454	5
Ndrg2	0	0.6043657	0.3	0.057	5
Flt1	0	0.5983766	0.194	0.007	5
Gpr37l1	0	0.589757	0.257	0.008	5
Slc6a11	0	0.583096	0.247	0.009	5
Aldoc1	0	0.5646454	0.446	0.353	5
Bcan	0	0.5470201	0.265	0.121	5
Gja1	0	0.5269379	0.231	0.01	5
Bsg	0	0.5178038	0.325	0.315	5
Cd811	0	0.4869174	0.331	0.179	5
Ttyh1	0	0.4798814	0.311	0.149	5
Fgfr3	0	0.4471816	0.187	0.003	5
Vtn	0	0.4422136	0.121	0.002	5
Mobp1	0	0.4404429	0.297	0.127	5
Ly6c1	0	0.4356071	0.124	0.002	5
Pla2g7	0	0.4336423	0.215	0.067	5
Htra1	0	0.4315661	0.179	0.03	5
Zbtb20	0	0.4251622	0.461	0.352	5
Mt1	0	0.4185149	0.184	0.03	5
Kcnj101	0	0.4136619	0.217	0.038	5
Slc7a10	0	0.4054401	0.161	0.006	5
Clu	0	0.3963422	0.271	0.229	5
Itih3	0	0.3954393	0.149	0.004	5
Glul1	0	0.3948758	0.261	0.088	5
Macf1	0	0.389849	0.47	0.415	5
Scd21	0	0.3857611	0.387	0.258	5
Qk1	0	0.3819904	0.29	0.098	5
Pbxip1	0	0.3818055	0.18	0.021	5
mt-Cytb1	0	0.3775106	0.488	0.461	5
Ntsr2	0	0.3774527	0.153	0.004	5
Son	0	0.3771165	0.412	0.339	5
Fth11	0	0.3770047	0.508	0.461	5
Ptprz1	0	0.3698997	0.192	0.043	5

Slc1a3	0	0.3642971	0.152	0.01	5
mt-Co1	0	0.3642065	0.42	0.417	5
Agt	0	0.362874	0.137	0.003	5
Gpm6b1	0	0.3461048	0.258	0.103	5
Slc6a1	0	0.3452291	0.178	0.053	5
Syne11	0	0.3415591	0.468	0.462	5
Acsl3	0	0.3359276	0.203	0.105	5
Lrp1	0	0.3327339	0.311	0.282	5
Slco1a4	0	0.3311611	0.121	0.003	5
Plpp3	0	0.3203941	0.14	0.009	5
Tril	0	0.3178307	0.144	0.01	5
Serpine2	0	0.314655	0.176	0.056	5
Epas1	0	0.3016294	0.138	0.02	5
Nnat	0	0.2996618	0.108	0.013	5
Rapgef3	0	0.2987869	0.139	0.014	5
Slc38a3	0	0.2909174	0.13	0.006	5
Utrn	0	0.2904571	0.183	0.077	5
Ptn1	0	0.2788613	0.188	0.103	5
Nwd1	0	0.2756162	0.139	0.049	5
Itm2a	0	0.2745194	0.106	0.01	5
mt-Nd5	0	0.2720926	0.393	0.406	5
Slc27a1	0	0.2688832	0.135	0.051	5
Sdc4	0	0.2600682	0.113	0.006	5
Slc2a1	0	0.2588932	0.116	0.015	5
Dbi	0	0.2564351	0.123	0.049	5
Trpm3	8.53350183497001e-320	0.3061331	0.192	0.073	5
Daam21	3.97E-303	0.2576742	0.14	0.045	5
Fn1	0	0.7072006	0.266	0.012	6
Sparcl13	0	0.6895945	0.797	0.45	6
Maf	0	0.5596038	0.514	0.051	6
Hcn1	0	0.5393843	0.518	0.134	6
Ndrg41	0	0.5139276	0.737	0.445	6
Nefh1	0	0.5119571	0.654	0.339	6
Nefm2	0	0.4980926	0.745	0.486	6
Lgi2	0	0.4844967	0.48	0.156	6
Ldhb2	0	0.4824331	0.651	0.33	6
Mafb	0	0.465526	0.401	0.014	6
Ckb2	0	0.4379359	0.713	0.437	6
Map1a2	0	0.4194278	0.711	0.455	6
Lpgat1	0	0.4122993	0.481	0.23	6
Hhip	0	0.4004197	0.216	0.009	6
Atp1b12	0	0.3793687	0.908	0.721	6
Spp1	0	0.3702855	0.351	0.073	6

Pcp4l1	0	0.3627434	0.436	0.194	6
Rap1gds1	0	0.3358917	0.323	0.112	6
Cd24a	0	0.3063732	0.247	0.028	6
Pvalb1	0	0.2977513	0.38	0.115	6
Sema7a	0	0.2931878	0.333	0.076	6
Lifr	0	0.2900475	0.338	0.089	6
Tcf4	0	0.2879863	0.429	0.154	6
Sphkap1	0	0.2814172	0.359	0.086	6
Rcan2	0	0.2679705	0.488	0.228	6
Gm205942	1.88E-254	0.3430948	0.789	0.618	6
Atp1a32	1.33E-253	0.3597125	0.721	0.506	6
mt-Nd11	4.26E-241	0.2693782	0.592	0.386	6
Nefl2	2.18E-227	0.3137003	0.573	0.374	6
Chgb1	0	0.7663805	0.7	0.3	7
Map1b1	0	0.5038042	0.855	0.706	7
Slc24a21	0	0.5022044	0.605	0.316	7
Snap252	0	0.4525786	0.806	0.627	7
Cplx21	0	0.4433372	0.47	0.131	7
Slc17a7	0	0.4349322	0.398	0.017	7
Pcp4	0	0.3590712	0.333	0.092	7
Gls	0	0.3527068	0.515	0.219	7
Sv2b	0	0.3437068	0.409	0.105	7
Spp11	0	0.3404474	0.342	0.074	7
Chd7	0	0.3316383	0.271	0.052	7
Syt1	0	0.3221465	0.462	0.178	7
Igfbp5	0	0.3151454	0.278	0.023	7
Zic1	0	0.2792836	0.206	0.016	7
Cpe	1.80E-266	0.2703337	0.543	0.315	7
Syne12	2.09E-265	0.3894454	0.669	0.456	7
Atp1b13	1.77E-261	0.3342662	0.864	0.723	7
Ndrg42	5.55E-236	0.3163572	0.644	0.448	7
Nefh2	1.86E-228	0.2723553	0.561	0.343	7
Dnm11	6.44E-223	0.3008523	0.552	0.347	7
Calm11	1.15E-216	0.3708707	0.794	0.667	7
Napb1	2.85E-207	0.2796105	0.631	0.447	7
Atp1a33	3.42E-125	0.2994903	0.661	0.509	7
Nefm3	0	1.7615498	0.976	0.485	8
Nefl3	0	1.680043	0.944	0.369	8
Map1b2	0	1.4496842	0.994	0.704	8
Nefh3	0	1.3304945	0.913	0.338	8
Slc5a7	0	0.9078166	0.65	0.011	8
Stmn2	0	0.9042521	0.808	0.399	8
Acly	0	0.8692583	0.702	0.146	8

Prune2	0	0.8525777	0.658	0.172	8
Calm12	0	0.8293291	0.946	0.665	8
S100b1	0	0.7708839	0.662	0.139	8
Sncg	0	0.7306761	0.582	0.061	8
Caln1	0	0.704289	0.649	0.18	8
Fgf1	0	0.6903476	0.619	0.087	8
Tppp31	0	0.6638242	0.554	0.088	8
Prph	0	0.6044724	0.522	0.007	8
Tubb3	0	0.5901334	0.642	0.245	8
Calm22	0	0.5212103	0.824	0.528	8
Pcp4l11	0	0.5067066	0.451	0.196	8
Vamp12	0	0.4938005	0.691	0.349	8
Atp1a1	0	0.4863912	0.422	0.067	8
mt-Nd12	0	0.4760841	0.697	0.387	8
Ahnak2	0	0.4678602	0.395	0.017	8
Ywhag1	0	0.4623602	0.693	0.374	8
Actg1	0	0.4526164	0.621	0.294	8
Epb41l3	0	0.4479075	0.651	0.376	8
Kif5c	0	0.447675	0.63	0.307	8
mt-Cytb2	0	0.4439124	0.764	0.456	8
Dffa	0	0.4280913	0.413	0.075	8
mt-Nd51	0	0.4186614	0.712	0.4	8
Rgs7bp1	0	0.4116456	0.514	0.2	8
Cplx12	0	0.4108131	0.737	0.41	8
Tns1	0	0.4064747	0.438	0.032	8
Fxyd7	0	0.4029779	0.326	0.021	8
Map2	0	0.4013043	0.633	0.336	8
Uchl1	0	0.3851554	0.546	0.253	8
Slc18a3	0	0.3789193	0.398	0.003	8
Sv2c1	0	0.3731882	0.504	0.211	8
Tuba1a1	0	0.3690301	0.575	0.261	8
Chodl	0	0.366018	0.296	0.012	8
Calca	0	0.3606921	0.244	0.004	8
Lgals1	0	0.3576738	0.297	0.011	8
Clu1	0	0.3558484	0.53	0.225	8
Slc7a14	0	0.3557184	0.459	0.125	8
Dkk3	0	0.3495818	0.366	0.053	8
Plec	0	0.348697	0.475	0.192	8
Fam135b	0	0.3239991	0.442	0.129	8
Ret	0	0.308943	0.366	0.046	8
Htra11	0	0.3034084	0.371	0.029	8
Fstl1	0	0.2988288	0.417	0.119	8
Rgs4	0	0.2960419	0.371	0.081	8

Capns1	0	0.2954707	0.395	0.118	8
Anxa6	0	0.2950323	0.412	0.111	8
Susd2	0	0.2771392	0.334	0.032	8
Fbxo2	0	0.2735682	0.363	0.108	8
Lifr1	0	0.2688005	0.359	0.091	8
Nfia	0	0.2673963	0.332	0.079	8
Stk32a	0	0.2630793	0.267	0.009	8
Kcnk9	0	0.2618339	0.409	0.129	8
Cyb5r3	0	0.2597222	0.327	0.046	8
Calcb	0	0.2563324	0.263	0.002	8
Endod1	0.00E+00	0.2885554	0.46	0.19	8
Rab6b	5.57E-307	0.3266993	0.532	0.248	8
Tuba1b	5.64E-302	0.3465961	0.576	0.295	8
Sptbn1	5.84E-296	0.3690503	0.662	0.395	8
mt-Co11	1.60E-295	0.3758191	0.707	0.412	8
Disp2	1.46E-285	0.4065246	0.573	0.323	8
Sorl1	2.44E-284	0.3597243	0.563	0.301	8
Hspa12a	1.09E-278	0.2626278	0.465	0.203	8
Klc1	7.90E-266	0.289986	0.532	0.263	8
mt-Nd6	2.09E-261	0.4164883	0.556	0.296	8
mt-Nd4	1.05E-258	0.3396292	0.524	0.261	8
Nars1	3.10E-256	0.3403952	0.616	0.349	8
mt-Nd21	5.33E-252	0.3968357	0.582	0.317	8
1110008P14Rik	1.02E-250	0.2538771	0.266	0.087	8
Hsp90aa11	5.63E-243	0.3770925	0.765	0.557	8
Map7d21	5.14E-231	0.3180183	0.623	0.362	8
Gm205943	8.43E-230	0.3632201	0.849	0.618	8
Kif21a	1.18E-229	0.3265865	0.641	0.403	8
Calm31	2.57E-227	0.3245775	0.625	0.37	8
Glra12	2.15E-217	0.2504803	0.528	0.279	8
Hsp90ab11	1.30E-192	0.2963025	0.801	0.615	8
Syt111	2.54E-185	0.3116977	0.759	0.553	8
Pkm1	1.46E-180	0.2980566	0.707	0.5	8
Pja2	1.51E-172	0.2607769	0.59	0.366	8
Stmn32	1.01E-169	0.3034142	0.623	0.399	8
Sptan1	1.01E-169	0.2879788	0.641	0.439	8
Ubb	3.79E-167	0.2748471	0.597	0.377	8
Kif5a	4.44E-167	0.2540981	0.617	0.396	8
Dync1h1	1.64E-140	0.2842837	0.633	0.444	8
Slc25a41	2.83E-138	0.2611627	0.726	0.524	8
Lars21	1.17E-80	0.3756277	0.948	0.86	8
Ttr	0	5.5248098	0.987	0.136	9
Enpp21	0	3.2458434	0.985	0.116	9

Trpm31	0	1.4798515	0.901	0.063	9
Apoe1	0	1.1665227	0.814	0.06	9
Arl6ip1	0	0.998859	0.823	0.342	9
Kl	0	0.9728218	0.7	0.017	9
mt-Nd52	0	0.8574512	0.865	0.398	9
Clu2	0	0.8504709	0.785	0.221	9
1500015O10Rik	0	0.8440248	0.621	0.001	9
Bsg1	0	0.8281743	0.813	0.307	9
Igfbp2	0	0.7614576	0.583	0.003	9
Prlr	0	0.7344926	0.574	0.034	9
Hspa5	0	0.7204849	0.817	0.365	9
mt-Nd61	0	0.6708455	0.722	0.293	9
Folr1	0	0.6515169	0.524	0.001	9
Clic6	0	0.6493874	0.496	0.002	9
Pbxip11	0	0.6342494	0.552	0.017	9
Cst31	0	0.5943275	0.595	0.154	9
Hsp90b1	0	0.5700656	0.72	0.34	9
Gm205944	0	0.5534777	0.909	0.618	9
Col9a3	0	0.5530513	0.451	0.005	9
F5	0	0.5422409	0.448	0.001	9
Kcnj13	0	0.5318642	0.444	0.001	9
Abhd2	0	0.5180168	0.367	0.032	9
Cd63	0	0.5174269	0.468	0.025	9
Calr	0	0.5089094	0.628	0.276	9
Slc4a2	0	0.5041416	0.495	0.071	9
Kcne2	0	0.499141	0.424	0	9
Sostdc1	0	0.4843245	0.4	0.001	9
Slc12a21	0	0.4646736	0.535	0.098	9
mt-Co12	0	0.4639086	0.739	0.411	9
Ptgds2	0	0.4631587	0.617	0.108	9
mt-Cytb3	0	0.4605701	0.783	0.456	9
Ace	0	0.4370415	0.303	0.021	9
Slc16a2	0	0.4338758	0.402	0.006	9
Car12	0	0.4242717	0.356	0.004	9
Slc4a10	0	0.4239848	0.445	0.117	9
Htr2c	0	0.4238085	0.431	0.086	9
Ctsd	0	0.4174925	0.462	0.117	9
Ezr	0	0.3879193	0.339	0.003	9
Lamb1	0	0.3734095	0.329	0.017	9
Cab39l	0	0.366835	0.374	0.048	9
Itpr1	0	0.3662083	0.366	0.067	9
Slc4a5	0	0.3541353	0.305	0.001	9
Col8a1	0	0.3474446	0.324	0.009	9

Cgnl1	0	0.3466997	0.325	0.083	9
Otx2	0	0.3452171	0.318	0.001	9
Slco1c1	0	0.3436034	0.312	0.005	9
Ifi27	0	0.3364907	0.333	0.032	9
Sparc1	0	0.3354434	0.378	0.039	9
Sod3	0	0.3312557	0.297	0.003	9
Wls	0	0.325979	0.326	0.022	9
Tbc1d9	0	0.3118417	0.311	0.068	9
Atp1a11	0	0.3046613	0.29	0.07	9
Rdh5	0	0.3028931	0.279	0.002	9
Slc13a4	0	0.3025639	0.282	0.013	9
Ccnd2	0	0.2963421	0.288	0.029	9
Ppp1r1b	0	0.2934323	0.262	0.005	9
Fxyd1	0	0.2914018	0.285	0.004	9
Dnajc3	0	0.2905242	0.35	0.091	9
Msx1	0	0.2867925	0.264	0.001	9
Cdkn1c	0	0.2862008	0.258	0.004	9
Slc31a1	0	0.2846267	0.271	0.016	9
Car21	0	0.279256	0.433	0.077	9
Mfrp	0	0.2777927	0.178	0.002	9
Sulf1	0	0.274706	0.243	0.006	9
Abca4	0	0.2708458	0.225	0.003	9
Stk39	0	0.2640549	0.306	0.088	9
Strip2	0	0.2632678	0.272	0.059	9
Syne2	0	0.2618109	0.258	0.019	9
Plxnb2	0	0.2608731	0.238	0.029	9
Col8a2	0	0.2550985	0.229	0.002	9
Cd59a	1.55595662130222e-314	0.2833584	0.392	0.136	9
mt-Nd41	4.38E-294	0.3260103	0.547	0.261	9
mt-Nd22	9.43E-292	0.3695885	0.61	0.317	9
Tmem721	6.24E-286	0.3403095	0.588	0.297	9
Zbtb201	2.44E-268	0.3166631	0.643	0.35	9
Eef1a11	5.14E-265	0.2800504	0.454	0.19	9
Psap	1.67E-257	0.3603301	0.621	0.358	9
Ahcyl2	3.56E-254	0.2552917	0.315	0.111	9
Slc22a17	6.91E-246	0.3033416	0.538	0.283	9
Atp2b3	4.32E-244	0.298423	0.34	0.152	9
Lars22	2.06E-80	0.4367687	0.956	0.86	9
Nrcam	0	1.2774311	0.788	0.224	10
Scn3a	0	1.101072	0.745	0.08	10
Slc1a21	0	0.730126	0.545	0.054	10
Rph3a1	0	0.6743113	0.589	0.239	10
Cacna1e	0	0.6706936	0.575	0.143	10

Calb1	0	0.6062498	0.466	0.031	10
Arpp211	0	0.5819031	0.547	0.145	10
Syt12	0	0.5563635	0.526	0.18	10
Crh	0	0.528979	0.354	0.009	10
Nell2	0	0.5176584	0.398	0.056	10
Msi2	0	0.5121358	0.514	0.189	10
Foxp2	0	0.5040948	0.425	0.029	10
Gpr88	0	0.4977039	0.372	0.002	10
Cplx22	0	0.4607197	0.449	0.135	10
Gpr26	0	0.4283786	0.347	0.027	10
Pex5l1	0	0.4144912	0.422	0.103	10
Htr5b	0	0.4015871	0.326	0.001	10
Plcxd2	0	0.3858854	0.362	0.089	10
Kit	0	0.3382917	0.293	0.016	10
Gabrg1	0	0.3347289	0.304	0.024	10
Pou4f1	0	0.3278475	0.292	0.006	10
Foxp1	0	0.3243898	0.308	0.054	10
Cacna1g	0	0.2996582	0.276	0.045	10
Kcng1	0	0.2746611	0.257	0.008	10
Cnih3	0	0.2632164	0.258	0.011	10
Ajap1	0	0.2603678	0.269	0.042	10
Lmo7	0	0.2591114	0.203	0.008	10
Dnah11	0	0.2583439	0.19	0.002	10
C1ql1	0	0.2538234	0.244	0.004	10
Smpd3	0	0.251076	0.26	0.038	10
Calb2	1.68970450877706e-321	0.3260941	0.349	0.081	10
Nav3	2.41207098104162e-314	0.3245279	0.334	0.079	10
Adgra1	2.52E-268	0.2809944	0.306	0.081	10
Kcnh7	5.64E-253	0.2745858	0.3	0.077	10
Zfp462	8.68E-233	0.2779432	0.313	0.091	10
Ptprd1	8.32E-229	0.4075489	0.598	0.315	10
Cpne6	6.30E-221	0.2523094	0.269	0.068	10
Fbxw7	4.04E-214	0.2960523	0.364	0.143	10
Pcp4l12	1.81E-213	0.3971873	0.41	0.198	10
Snhg111	5.51E-206	0.496118	0.978	0.863	10
Kmt2c	1.72E-190	0.3067879	0.396	0.161	10
Gpm6a	5.23E-187	0.2938516	0.395	0.164	10
Tsc22d1	2.12E-182	0.2741192	0.358	0.157	10
Lgi21	6.29E-168	0.2698586	0.357	0.163	10
Cntnap2	1.25E-139	0.2832811	0.435	0.251	10
Akap6	1.42E-131	0.2875968	0.414	0.24	10
Ntrk3	1.88E-125	0.2500144	0.399	0.204	10
Rab3c	5.80E-123	0.2532833	0.422	0.231	10

Zbtb202	1.67E-73	0.2667237	0.503	0.353	10
Nat8l1	0	1.7055516	0.764	0.277	11
Stx1b	0	1.0309443	0.694	0.299	11
Lars23	0	0.9530447	0.951	0.86	11
Vmn1r206	0	0.8928626	0.557	0.024	11
Spock2	0	0.797972	0.691	0.39	11
Fyco1	0	0.7464235	0.556	0.129	11
Dcbld2	0	0.6233987	0.43	0.052	11
Mtch1	0	0.6186533	0.497	0.223	11
Spop	0	0.5920649	0.5	0.191	11
Dynll2	0	0.579814	0.543	0.339	11
Srgap3	0	0.5705221	0.511	0.219	11
Ctnnd2	0	0.488252	0.413	0.129	11
Cd22	0	0.4447912	0.27	0.01	11
Tgfbi	0	0.3447108	0.229	0.025	11
Abcc4	0	0.3030108	0.197	0.012	11
Rgs51	0	0.2544776	0.191	0.011	11
Mdga2	7.34132143155508e-319	0.4749736	0.429	0.165	11
Usp53	1.51E-303	0.3861844	0.298	0.065	11
Shq1	5.82E-281	0.3338673	0.241	0.045	11
Lonrf1	1.02E-274	0.3610977	0.287	0.072	11
Fam219a	1.57E-273	0.357584	0.324	0.111	11
Slc16a10	9.07E-271	0.3423832	0.247	0.05	11
Shld1	1.83E-248	0.2934787	0.204	0.035	11
Tmem132d	1.55E-246	0.281562	0.199	0.03	11
Arf3	1.18E-244	0.3719308	0.389	0.182	11
Lhfpl4	7.28E-242	0.3507863	0.32	0.117	11
Slc9b2	4.73E-232	0.26379	0.192	0.029	11
Mrgpre	1.63E-229	0.264325	0.197	0.034	11
Pik3c2a	3.39E-210	0.3078433	0.265	0.072	11
Madd	2.06E-202	0.3710589	0.391	0.204	11
Fam160b2	3.69E-199	0.3052518	0.265	0.082	11
Mroh1	2.08E-188	0.3731423	0.375	0.183	11
Dzank1	2.94E-147	0.3014214	0.406	0.259	11
Celf41	6.04E-135	0.3726442	0.456	0.3	11
Gdi1	4.88E-116	0.2742928	0.465	0.343	11
Atp1a34	3.48E-99	0.3178588	0.663	0.511	11
Pkd1	1.79E-89	0.2681207	0.362	0.205	11
Slc6a51	0	1.0958838	0.891	0.156	12
Sparcl14	0	1.0323294	0.97	0.455	12
Spp12	0	0.9663713	0.864	0.074	12
Ndrg43	0	0.8950686	0.942	0.449	12
Map1a3	0	0.8822419	0.947	0.458	12

Nefh4	0	0.8305947	0.928	0.343	12
Ckb3	0	0.8289576	0.939	0.441	12
Calb11	0	0.7896467	0.714	0.031	12
Lamp51	0	0.7547427	0.878	0.216	12
Gm205945	0	0.6930772	0.954	0.62	12
Atp1b14	0	0.6395438	0.99	0.725	12
mt-Cytb4	0	0.6235564	0.925	0.458	12
Nefm4	0	0.6133711	0.947	0.49	12
Ldhb3	0	0.6117885	0.872	0.335	12
mt-Co13	0	0.6095623	0.901	0.413	12
mt-Nd13	0	0.6000307	0.862	0.389	12
Cd24a1	0	0.5902107	0.63	0.029	12
mt-Nd53	0	0.5291358	0.872	0.402	12
Pcp4l13	0	0.517397	0.702	0.197	12
Cplx13	0	0.5102504	0.908	0.411	12
Doc2g	0	0.5027164	0.436	0.007	12
Kcnc31	0	0.4906735	0.805	0.276	12
Ttn	0	0.4816575	0.447	0.025	12
Sv2c2	0	0.4757905	0.744	0.212	12
Pvalb2	0	0.423102	0.605	0.118	12
Fgf11	0	0.4163892	0.618	0.092	12
Kcna11	0	0.4152854	0.804	0.295	12
Ina2	0	0.4123801	0.75	0.278	12
Vamp13	0	0.4072803	0.847	0.351	12
Rcan21	0	0.4012657	0.736	0.231	12
Nrxn3	0	0.3821606	0.872	0.376	12
Dner	0	0.3754797	0.638	0.129	12
Lpgat11	0	0.3600748	0.691	0.234	12
Lgi22	0	0.3555206	0.638	0.162	12
Ghitm1	0	0.3490615	0.812	0.345	12
Syt21	0	0.3391313	0.82	0.332	12
Tenm4	0	0.333517	0.638	0.194	12
Pacsin2	0	0.3125246	0.59	0.113	12
Elovl5	0	0.3066045	0.52	0.07	12
Rgs7bp2	0	0.2964391	0.644	0.202	12
Hspg2	0	0.2742651	0.314	0.005	12
Ttll7	0	0.2647731	0.674	0.235	12
Mdh11	2.27270197086973e-322	0.4502565	0.846	0.394	12
Scn8a1	3.4090529563046e-322	0.2820236	0.788	0.343	12
mt-Nd42	9.78249978765668e-322	0.3718868	0.713	0.262	12
Atp2a21	1.82557256138341e-320	0.3863988	0.829	0.372	12
Scn4b1	4.67703923514476e-315	0.2729264	0.532	0.143	12
Atp1a35	6.29094088921395e-314	0.7133905	0.916	0.509	12

Psap1	1.12E-307	0.2925393	0.797	0.359	12
Clstn11	5.22E-305	0.3281631	0.806	0.364	12
Cend1	5.78E-305	0.2533888	0.665	0.244	12
Pkm2	4.74E-304	0.4148134	0.919	0.5	12
Atp5b2	6.34E-300	0.4577356	0.9	0.493	12
Myo5a	2.58E-298	0.2777	0.73	0.299	12
mt-Nd23	1.55E-297	0.5236348	0.75	0.319	12
Ywhag2	1.97E-292	0.2905228	0.805	0.376	12
Map1b3	1.72E-290	0.445745	0.982	0.707	12
Ctsb	2.54E-289	0.2507843	0.811	0.393	12
Glra13	4.36E-281	0.3094168	0.701	0.28	12
Aplp2	2.13E-271	0.2744142	0.828	0.42	12
Kcnc1	2.02E-268	0.3417431	0.754	0.335	12
Nars2	3.36E-263	0.2620816	0.753	0.351	12
Dnm12	5.51E-262	0.2891962	0.75	0.349	12
Snap253	2.92E-260	0.398959	0.968	0.629	12
Map7d22	2.46E-258	0.2653492	0.764	0.364	12
mt-Nd62	1.05E-251	0.4035462	0.701	0.297	12
Spock21	9.19E-251	0.337828	0.791	0.39	12
Slc25a42	8.21E-242	0.4874889	0.89	0.525	12
Hspa81	3.03E-235	0.4084137	0.837	0.452	12
Stmn33	1.58E-198	0.2987345	0.759	0.4	12
Dst	1.34E-193	0.2957473	0.888	0.553	12
Hsp90ab12	3.86E-187	0.2540817	0.926	0.616	12
Calm13	7.61E-138	0.2601454	0.925	0.668	12
Lars24	2.81E-90	0.3582159	0.991	0.86	12
Gapdh1	4.79E-87	0.3209065	0.657	0.415	12
Atp2b1	0	1.1125109	0.625	0.332	13
Grid2	0	1.0873093	0.651	0.074	13
Prkcd	0	0.8157546	0.392	0.01	13
Anks1b	0	0.7601955	0.502	0.111	13
Cdh6	0	0.7054873	0.442	0.042	13
Bod1l	0	0.7023377	0.473	0.203	13
Car8	0	0.6920567	0.313	0.015	13
Dgkh	0	0.6657198	0.447	0.054	13
Ryr1	0	0.6467085	0.304	0.007	13
Adarb2	0	0.5900202	0.381	0.051	13
Gria21	2.31173315689119e-319	0.7093644	0.654	0.418	13
Itpr11	9.17E-304	0.5869735	0.341	0.07	13
Grm1	3.61E-232	0.465593	0.358	0.128	13
Tnr	3.05E-228	0.552817	0.388	0.127	13
Ogfrl1	8.27E-190	0.408877	0.286	0.087	13
Cttnbp2	3.02E-181	0.4664438	0.376	0.118	13

Trim9	8.27E-173	0.4336005	0.343	0.124	13
Sptbn2	2.22E-171	0.4270163	0.328	0.135	13
Map4	4.48E-164	0.4223111	0.389	0.218	13
Kalrn	6.16E-147	0.4103535	0.361	0.127	13
Vav3	8.41E-141	0.2847696	0.196	0.033	13
Shank2	8.55E-141	0.3175443	0.227	0.045	13
Rora	7.23E-140	0.3847959	0.317	0.126	13
Snhg112	8.93E-140	0.5868579	0.973	0.863	13
Pcp41	1.67E-131	0.4350893	0.254	0.097	13
Thsd7a	1.75E-129	0.3622019	0.315	0.129	13
Rreb1	5.88E-129	0.2867385	0.178	0.025	13
Grin2b	5.23E-124	0.36892	0.32	0.149	13
Rasa4	8.78E-103	0.2659244	0.194	0.041	13
Tshz2	1.56E-99	0.3142172	0.249	0.099	13
Sorl11	1.05E-95	0.3516879	0.445	0.305	13
Inpp5j	1.31E-94	0.2978166	0.244	0.088	13
Ywhah	4.16E-94	0.2638047	0.327	0.289	13
Exoc6b	5.67E-94	0.302147	0.26	0.114	13
Sipa1l3	1.03E-88	0.2577282	0.22	0.066	13
Frmd4a	1.33E-85	0.3317603	0.307	0.144	13
Cdc42bpa	7.50E-85	0.3280913	0.363	0.204	13
Nsg1	2.60E-83	0.2624021	0.323	0.236	13
Auts2	2.50E-79	0.3059808	0.284	0.128	13
Kcnma1	1.95E-74	0.2800633	0.303	0.157	13
Cpe1	5.51E-68	0.2531741	0.381	0.321	13
Shank1	1.09E-65	0.3032743	0.388	0.269	13
Arhgef12	2.15E-60	0.258207	0.299	0.213	13
Unc80	4.36E-57	0.2639798	0.442	0.349	13
Ccdc88a	9.44E-56	0.2786791	0.314	0.199	13
Ndrg44	2.94E-49	0.260818	0.516	0.453	13
Tnr1	0	1.3532412	0.605	0.125	14
Nfasc1	0	1.2924187	0.454	0.267	14
Gjc31	0	1.0037385	0.424	0.046	14
Vcan	0	0.9512637	0.39	0.017	14
Frmd4a1	0	0.9455795	0.38	0.144	14
Sirt21	0	0.912696	0.386	0.08	14
Ptprz11	0	0.8346418	0.349	0.046	14
Gpr17	0	0.8178256	0.272	0.002	14
Marcks	0	0.7985201	0.325	0.045	14
Bcas1	0	0.7610374	0.284	0.016	14
Pdgfra	0	0.7543389	0.215	0.005	14
Ppfibp1	0	0.6943152	0.309	0.019	14
Fyn	0	0.6609994	0.283	0.053	14

Tns3	0	0.6198661	0.267	0.014	14
Itpr2	0	0.5977648	0.265	0.03	14
Cspg4	0	0.5137608	0.172	0.003	14
Bcan1	1.97626258336499e-323	0.7251053	0.354	0.125	14
Kank1	1.90E-293	0.4255857	0.187	0.009	14
Qk2	9.25E-287	0.8312374	0.447	0.102	14
Mbp2	2.92E-278	1.0087408	0.477	0.186	14
Enpp6	1.38E-270	0.5392537	0.217	0.013	14
Neu4	2.51E-259	0.3235842	0.12	0.001	14
Cd812	4.36E-259	0.6383522	0.38	0.183	14
Lrp11	1.81E-244	0.5703849	0.29	0.283	14
Tcf7l2	1.84E-238	0.3672304	0.155	0.006	14
Gpr37l11	1.03E-235	0.4903116	0.221	0.015	14
Plp11	2.14E-211	0.9779335	0.606	0.268	14
Plxnb31	1.15E-209	0.5915398	0.22	0.021	14
Mical3	2.62E-203	0.4841772	0.276	0.146	14
Cnp1	5.46E-203	0.8255272	0.363	0.081	14
Slc44a11	5.84E-199	0.48689	0.229	0.05	14
Cntn1	7.03E-194	0.3477394	0.316	0.286	14
Serpine21	1.04E-189	0.463918	0.22	0.059	14
Mpzl1	1.41E-189	0.3449105	0.15	0.01	14
Olig11	4.60E-189	0.4088429	0.187	0.014	14
Epn2	9.90E-189	0.4566033	0.219	0.044	14
Cemip2	2.33E-185	0.3978554	0.134	0.03	14
Sema4d	1.45E-180	0.41474	0.179	0.036	14
Sulf2	4.26E-180	0.3866972	0.185	0.042	14
Dock91	4.39E-177	0.510572	0.319	0.15	14
Cacng4	5.23E-176	0.3660899	0.146	0.022	14
Col9a31	1.29E-170	0.3352737	0.147	0.012	14
Epb41l2	1.18E-160	0.3857107	0.159	0.033	14
Tuba1a2	1.85E-158	0.366908	0.283	0.267	14
Xylt1	4.04E-158	0.3290188	0.132	0.024	14
Pik3r3	1.40E-156	0.3150863	0.127	0.039	14
Nav1	1.36E-155	0.3990551	0.293	0.201	14
Acsl31	1.17E-154	0.3782013	0.203	0.107	14
Trio	9.01E-153	0.3681115	0.271	0.19	14
Cd9	1.13E-148	0.2927605	0.117	0.009	14
Pcdh17	8.08E-146	0.3445803	0.202	0.141	14
Sema5a	1.58E-144	0.3585588	0.206	0.089	14
Ankrd281	1.10E-143	0.3999173	0.217	0.074	14
Olig2	1.82E-141	0.2793114	0.115	0.006	14
Mag1	7.97E-140	0.842908	0.325	0.09	14
Hip1r	1.93E-138	0.3327983	0.168	0.063	14

Sema6a	1.83E-137	0.3602354	0.171	0.049	14
Map4k4	1.36E-136	0.3920935	0.228	0.085	14
Son1	1.45E-134	0.332694	0.365	0.341	14
Arhgap31	4.74E-134	0.3162263	0.146	0.037	14
Col11a2	5.33E-134	0.3590702	0.139	0.017	14
Zeb21	5.40E-131	0.4512218	0.258	0.069	14
Rictor	1.18E-130	0.3471	0.194	0.09	14
Dock4	6.96E-129	0.3447094	0.194	0.092	14
Shisal1	7.16E-129	0.2685024	0.133	0.029	14
Ddx5	5.10E-126	0.3043107	0.369	0.365	14
Spon1	8.68E-120	0.2981022	0.145	0.043	14
Adamts41	1.20E-119	0.3744926	0.165	0.025	14
Hnrnpa2b1	2.40E-118	0.2546692	0.285	0.308	14
Ctsl	1.73E-116	0.2567533	0.146	0.082	14
Pcdh15	4.87E-116	0.2923265	0.137	0.059	14
Lcorl	6.19E-116	0.2605945	0.131	0.024	14
Fryl	3.37E-115	0.3081083	0.219	0.154	14
Nckap5	1.19E-114	0.2552841	0.13	0.025	14
Actb1	3.81E-109	0.3534303	0.524	0.528	14
Phldb11	2.18E-108	0.3369088	0.176	0.03	14
Chn2	1.57E-105	0.2714967	0.12	0.024	14
Man2a2	2.15E-104	0.285966	0.187	0.127	14
Sep-71	1.19E-102	0.2532509	0.287	0.292	14
Ncor2	2.04E-97	0.2801186	0.18	0.115	14
Ncam1	3.84E-96	0.2623187	0.334	0.331	14
Cldn111	1.45E-87	0.3507074	0.161	0.029	14
Kndc11	1.86E-84	0.2644373	0.19	0.174	14
Ugt8a1	1.01E-83	0.359458	0.206	0.066	14
Zbtb203	2.13E-82	0.253466	0.341	0.355	14
Utp14b	4.49E-82	0.2556812	0.131	0.048	14
Secisbp2l1	7.37E-82	0.2839502	0.153	0.071	14
Scd22	1.10E-73	0.3693815	0.382	0.262	14
Myrf1	1.12E-73	0.2602219	0.139	0.033	14
Tmeff21	1.98E-71	0.2624986	0.172	0.085	14
AC149090.11	2.41E-70	0.2727262	0.331	0.34	14
S100b2	6.01E-68	0.3718325	0.253	0.147	14
Aatk1	1.27E-65	0.2534311	0.175	0.117	14
Ptma1	1.10E-62	0.2533219	0.202	0.149	14
Sparc2	1.64E-57	0.3038959	0.15	0.044	14
Slc12a22	3.45E-47	0.277781	0.199	0.105	14
Mobp2	3.04E-30	0.3282238	0.22	0.132	14

Figures and figure supplements

The E3 ubiquitin ligase RNF220 maintains hindbrain *Hox* expression patterns through regulation of WDR5 stability

Huishan Wang et.al.

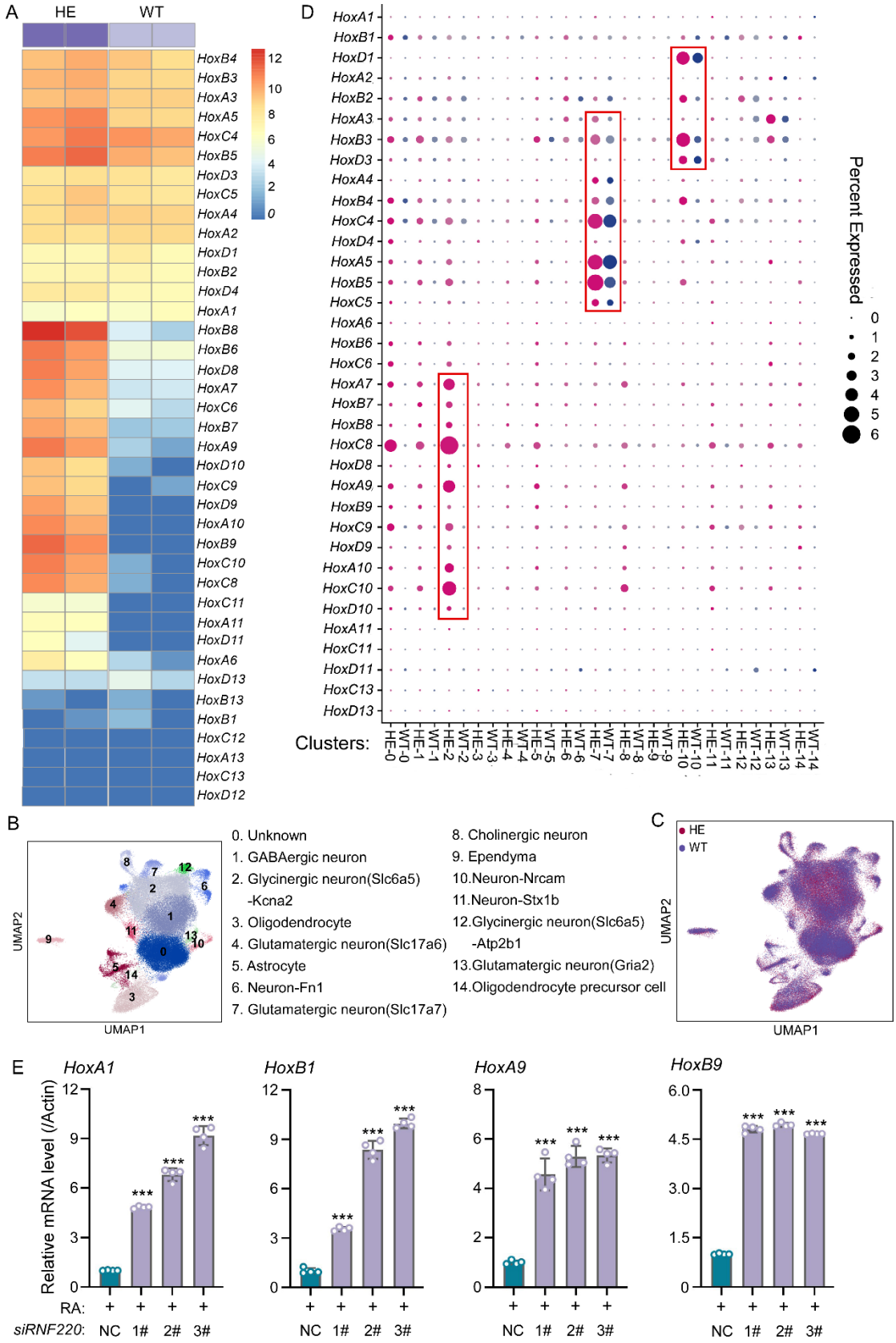

Figure 1. Up-regulation of *Hox* genes in pons of *Rnf220*$^{+/-}$ mice. (**A**) The heatmap of RNA-seq data showing *Hox* genes expression in pons of WT or *Rnf220*$^{+/-}$ mice (n=2 mice per group). (**B-C**) UMAP diagram showing 15 identified cell clusters annotated

by snRNA-seq analysis of pons. Each dot represents a single cell, and cells are laid out to show similarities (n=3 mice per group). (**D**) Heatmap of snRNA-seq data showing *Hox* expression changes in each cell cluster. (**E**) Quantitative real time polymerase chain reaction, qRT-PCR) analysis showing mRNA levels of indicated *Hox* genes in P19 cells when endogenous *Rnf220* was knocked down by siRNAs in the presence of RA. WT, wild-type. HE, heterozygote. RA, retinoic acid. $^{**}p < 0.01$, $^{***}p < 0.001$.

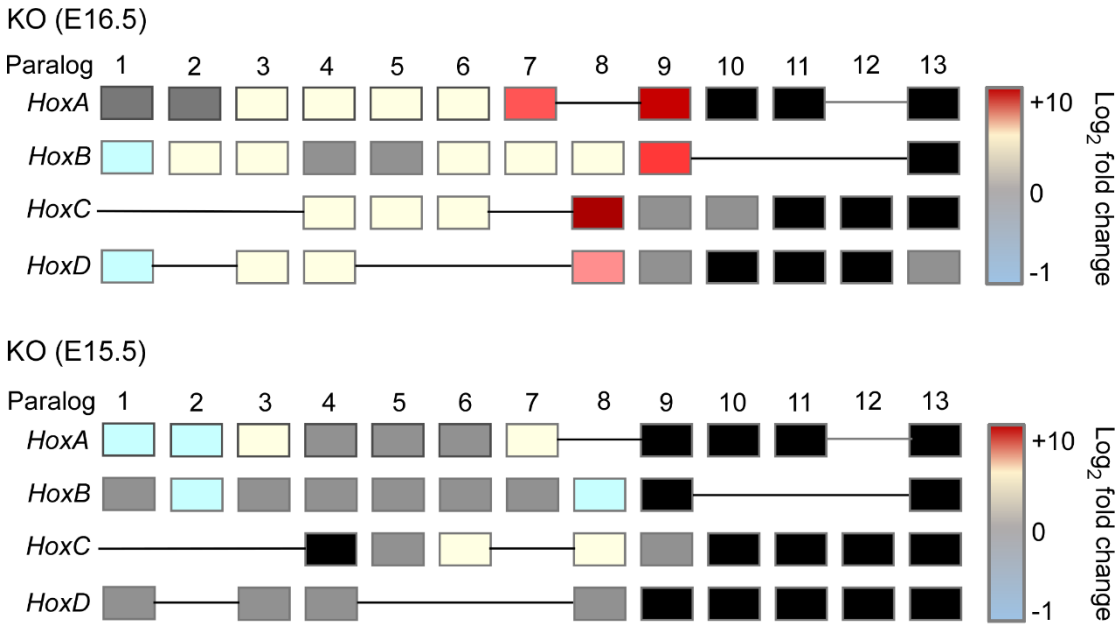

Figure 1-figure supplement 1. *Hox* genes exhibited de-repression in hindbrain of *Rnf220*$^{-/-}$ and *Rnf220*$^{+/-}$ mouse embryos at late developmental stages. Heatmap of *Hox* expression in hindbrain of *Rnf220*$^{-/-}$ mouse embryos at E16.5 and E15.5. Expression of each *Hox* gene was analyzed by qRT-PCR against GAPDH. Each *Hox* gene in wild-type controls was set to 1 (n=2 mice per group). Blank color represents the expression of that *Hox* is low and exceed detection range. KO, knockout.

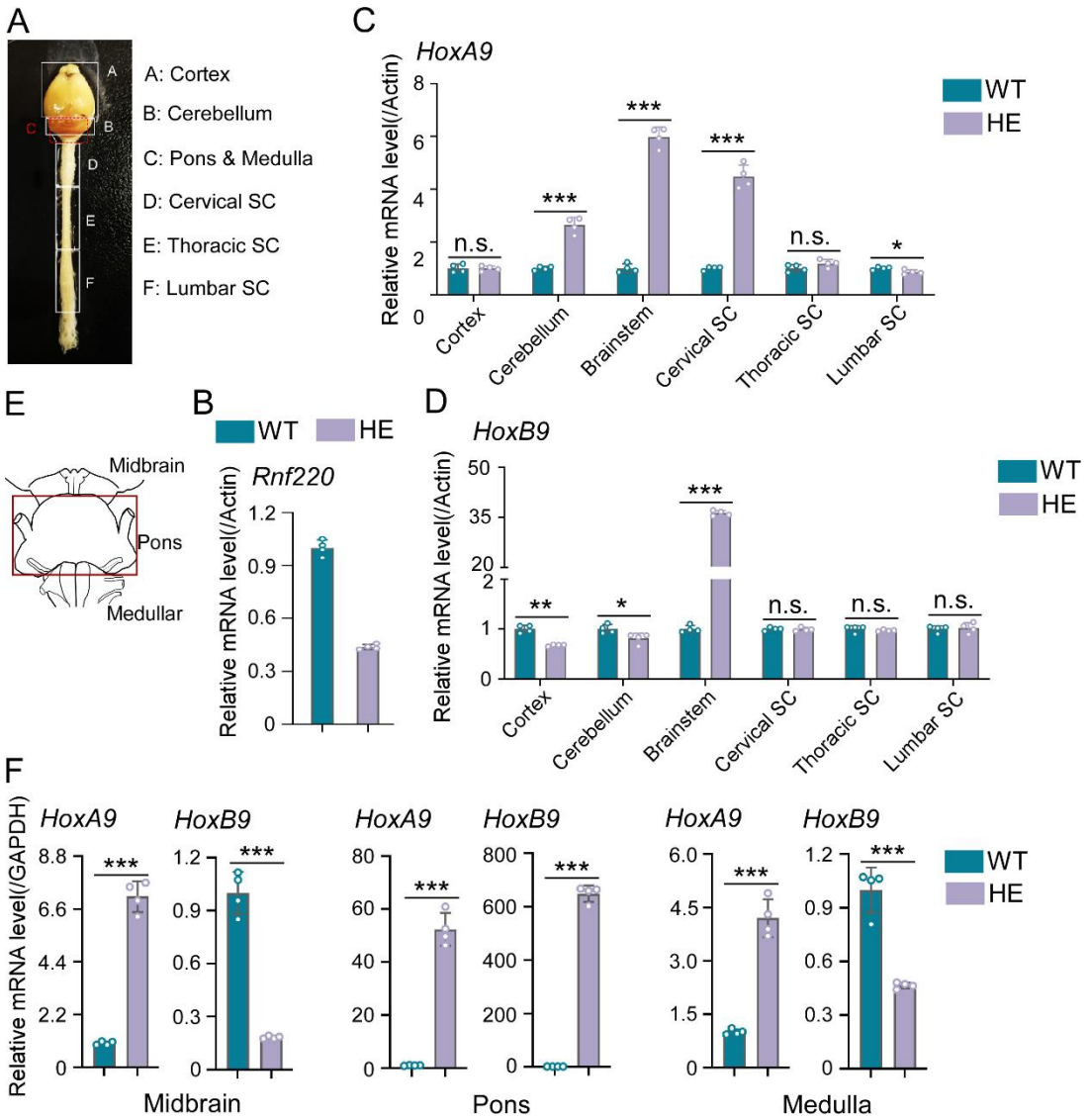

Figure 1-figure supplement 2. *Hox* genes were up-regulated in brainstem of *Rnf220*$^{+/-}$ mice. (**A**) Diagram of central neural system (CNS) in mice. (**B**) qRT-PCR analysis of *Rnf220* expression in CNS of *Rnf220*$^{+/-}$ and control mice. (**C-D**) qRT-PCR analysis of *HoxA9* (C) and *HoxB9* (D) expression in each CNS section of *Rnf220*$^{+/-}$ and control mouse. (**E**) Diagram of mouse brain stem. (**F**) qRT-PCR analysis of mRNA levels of *HoxA9* and *HoxB9* in indicated sections of WT and *Rnf220*$^{+/-}$ mouse brainstems (n=2 mice per group). WT, wild-type. HE, heterozygote. SC, Spinal cord. n.s., not significant. *$p < 0.05$, **$p < 0.01$, ***$p < 0.001$.

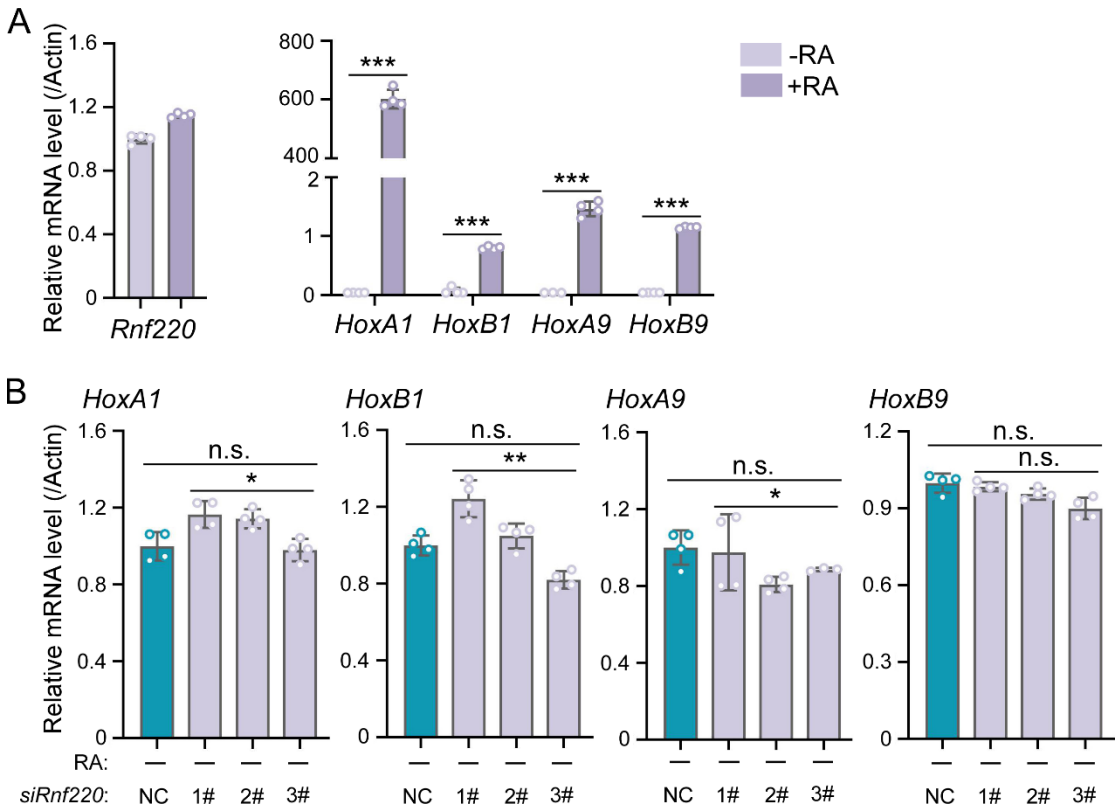

Figure 1-figure supplement 3. Expression levels of *Hox* genes were not affected by *Rnf220* knockdown in P19 cell line without RA induction. (**A**) qRT-PCR analysis of *Rnf220* and indicated *Hox* genes expression after RA treatment in P19 cells. (**B**) qRT-PCR analysis of expression levels of *HoxA1*, *HoxB1*, *HoxA9*, and *HoxB9* in *Rnf220* knockdown P19 cells without RA induction. RA: retinoic acid. n.s., not significant. *$p < 0.05$, **$p < 0.01$, ***$p < 0.001$.

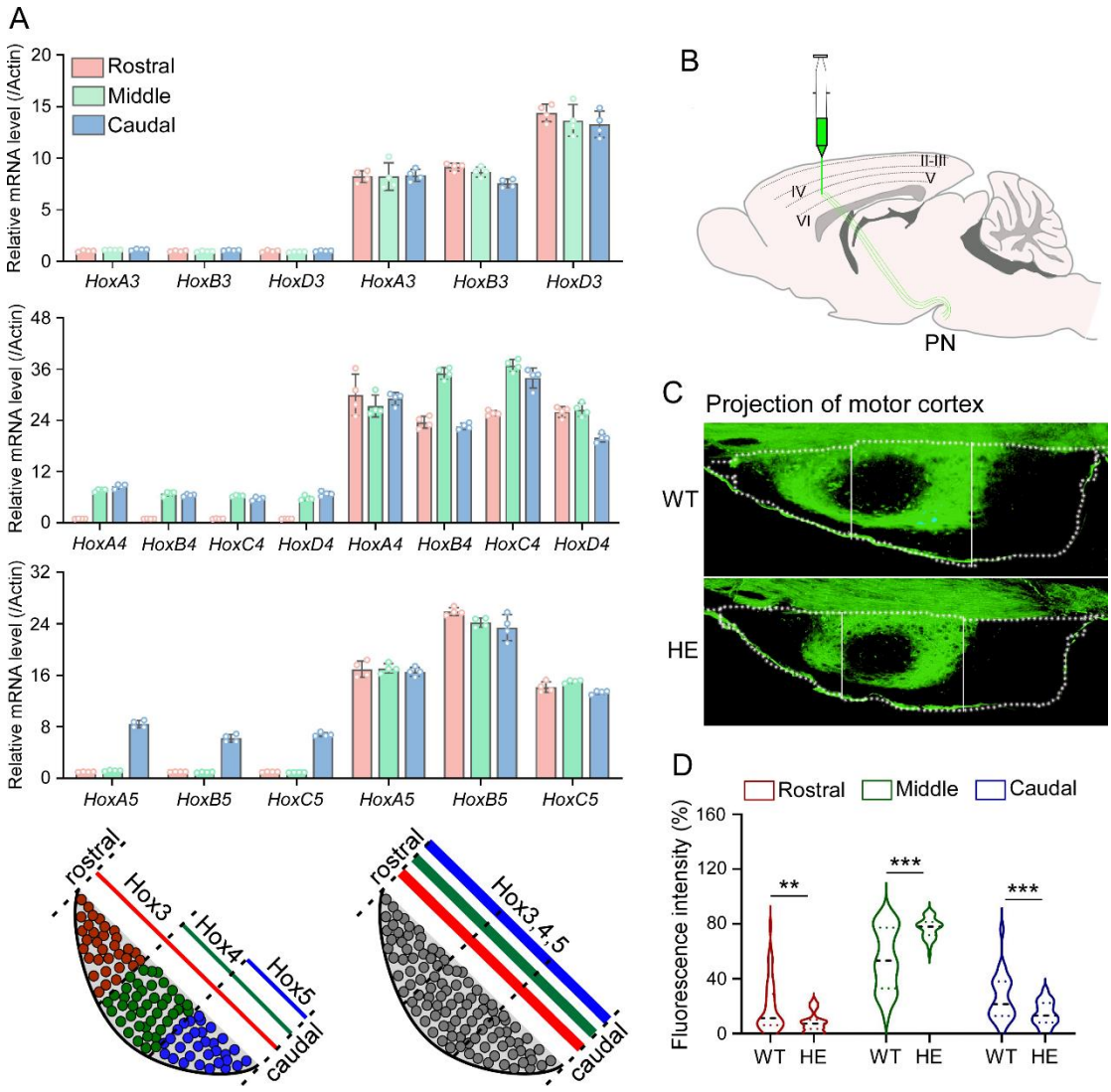

Figure 2. *Hox* gene expression was dysregulated and motor cortex projections were disorganized in PN of *Rnf220*$^{+/-}$ mice. (**A**) qRT-PCR analysis of relative expression levels of *Hox3*, *Hox4*, and *Hox5* in rostral, middle, and caudal sections of PN in WT and *RNF220*$^{+/-}$ mice. Expression level of each gene in rostral section of WT PN was set to 1. (n=4 mice per group). (**B**) Diagram of experimental stereotactic injections. (**C, D**) Fluorescent signals showing projection from motor cortex to PNs in WT and *Rnf220*$^{+/-}$ mice (n=2 mice per group). WT, wild-type; HE, heterozygote; $^{**}p < 0.01$; $^{***}p < 0.001$.

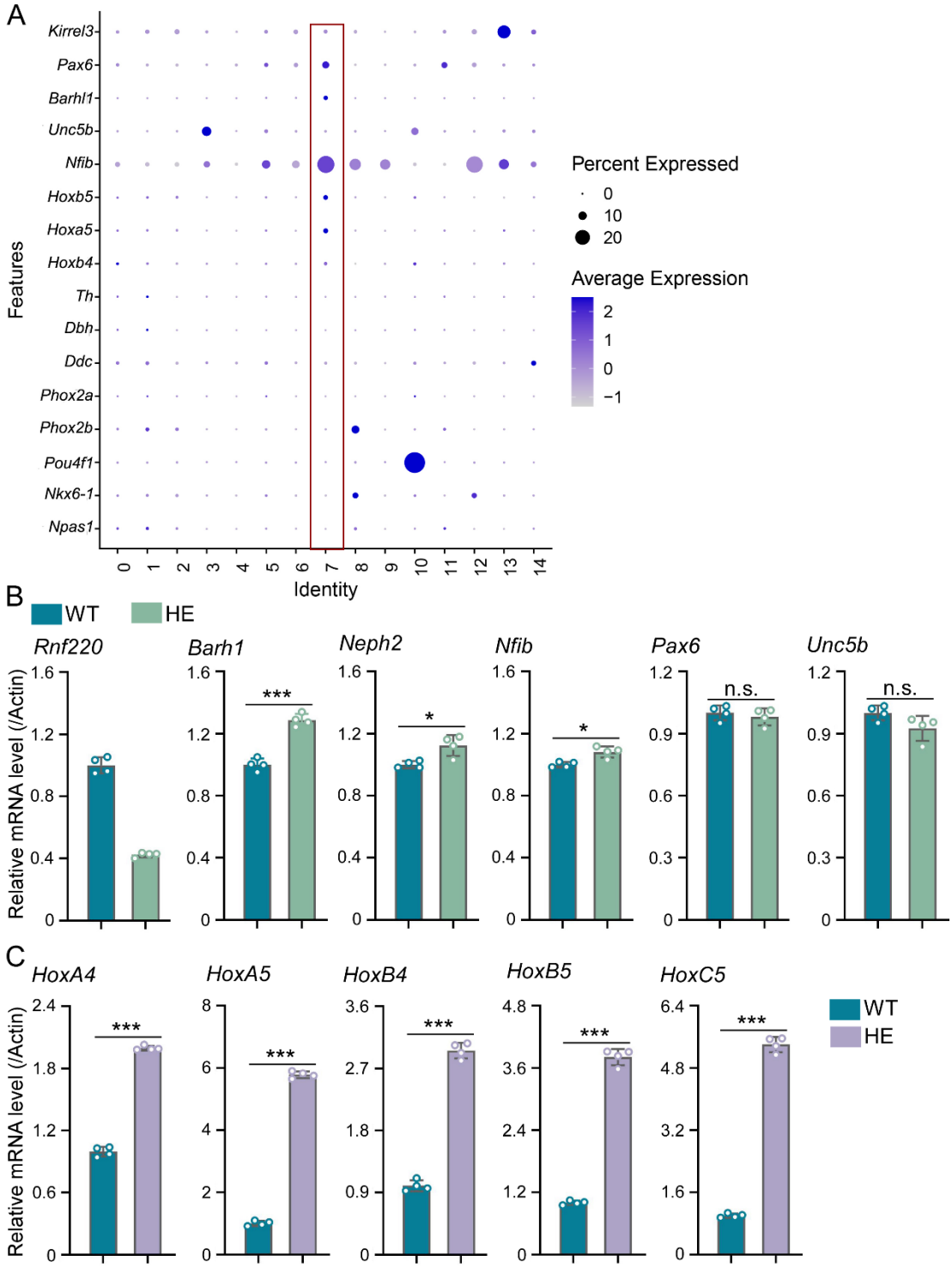

Figure 2-figure supplement 1. *Hox* genes were up-regulated in PN of *Rnf220*$^{+/-}$ mice. (**A**) Heatmap of snRNA-seq data showing expression levels of PN markers (*Pax6,*

Barhl1, *Unc5b*, and *Nfib*) among 15 identified cell clusters. (**B, C**) qRT-PCR analysis of expression levels of indicated PN markers (B) and *Hox* genes (C) in PN of *Rnf220*$^{+/-}$ and WT mice (n= 3 mice per group). WT, wild-type. HE, heterozygote. n.s., not significant. *$p < 0.05$, ***$p < 0.001$.

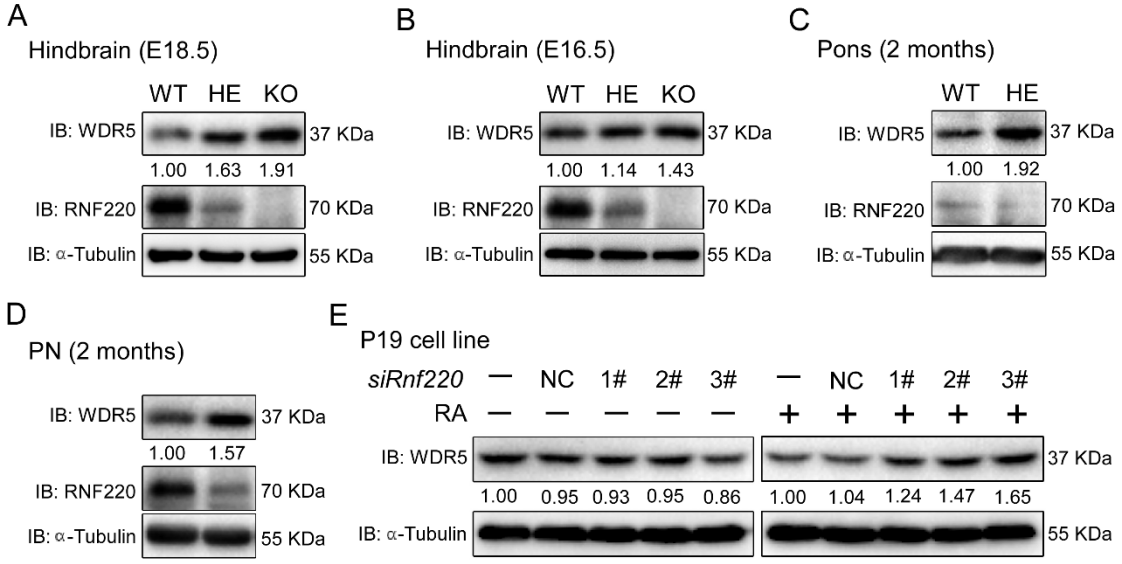

Figure 3. RNF220 mediates WDR5 degradation. **(A-D)** Western blots analysis showing the protein level of WDR5 in the indicated brain tissues of mice with different genotypes at different ages. **(E)** Western blot analysis of protein levels of WDR5 in P19 cells with *Rnf220* knockdown or not in the presence or absence of RA. IB, immunoblot. WT, wild-type. HE, heterozygote. KO, knockout. PN, pontine nuclei. NC, negative control. RA, retinoic acid.

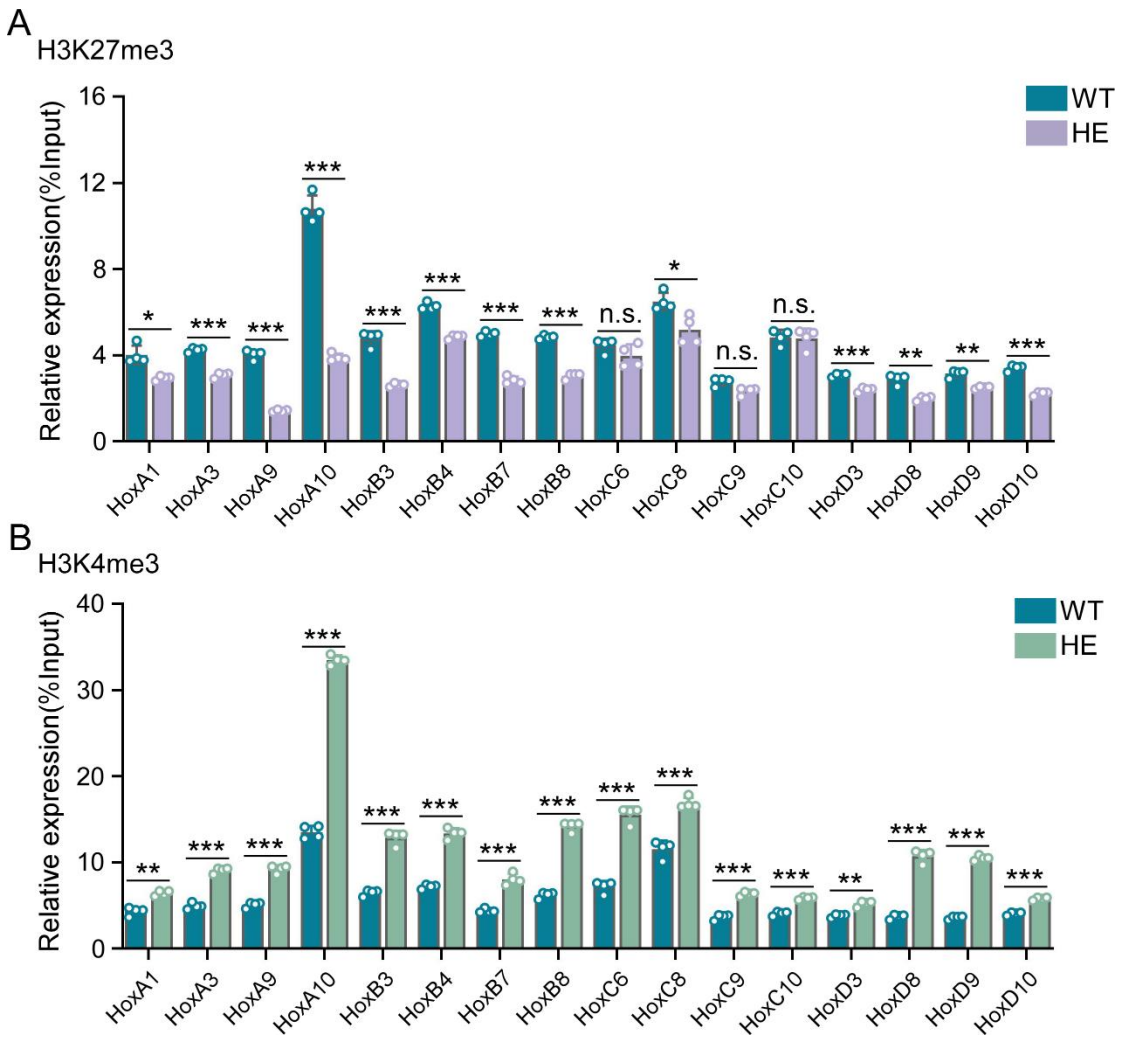

Figure 3-figure supplement1. Repressive epigenetic modification was down-regulated while activated epigenetic modification was up-regulated in promoter regions of indicated *Hox* genes in hindbrains of *Rnf220*$^{+/-}$ mice. **(A-B)** ChIP-qRT-PCR analysis of repressive epigenetic modification (H3K27me3) (A) and activated epigenetic modification (H3K4me3) (B) levels in promoter regions of indicated *Hox* genes in hindbrains of *Rnf220*$^{+/-}$ and WT mice (n=2 mice per group). WT, wild-type. HE, heterozygote. n.s., not significant. *p< 0.05, **p < 0.01, ***p < 0.001.

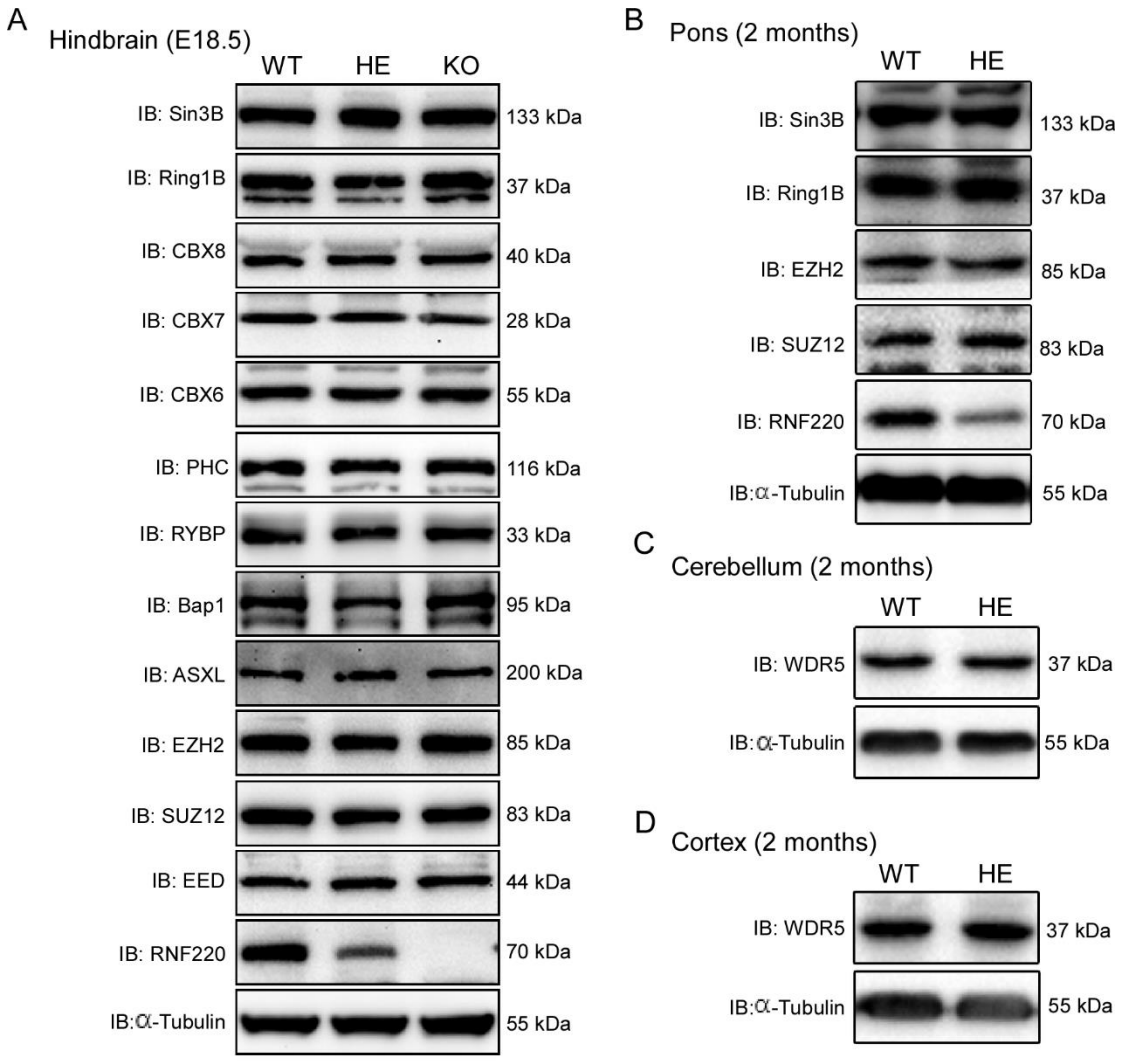

Figure 3-figure supplement 2. Protein levels of the indicated core components of PRC1 and PRC2 complex in indicated mouse brain tissues of different genotypes. (**A**) Western blot analysis of protein levels of core components of PRC1 and PRC2 complexes in hindbrain of WT, *Rnf220*$^{+/-}$, and *Rnf220*$^{-/-}$ mouse embryos at E18.5. (**B**) Western blot analysis of protein levels of core components of PRC1 and PRC2 complexes in pons of adult *Rnf220*$^{+/-}$ and WT mice. (**C, D**) Western blot analysis of protein levels of WDR5 in cerebellum and cortex of adult *Rnf220* $^{+/-}$ and WT mice. WT, wild-type; HE, heterozygote; KO, knockout; IB, immunoblot.

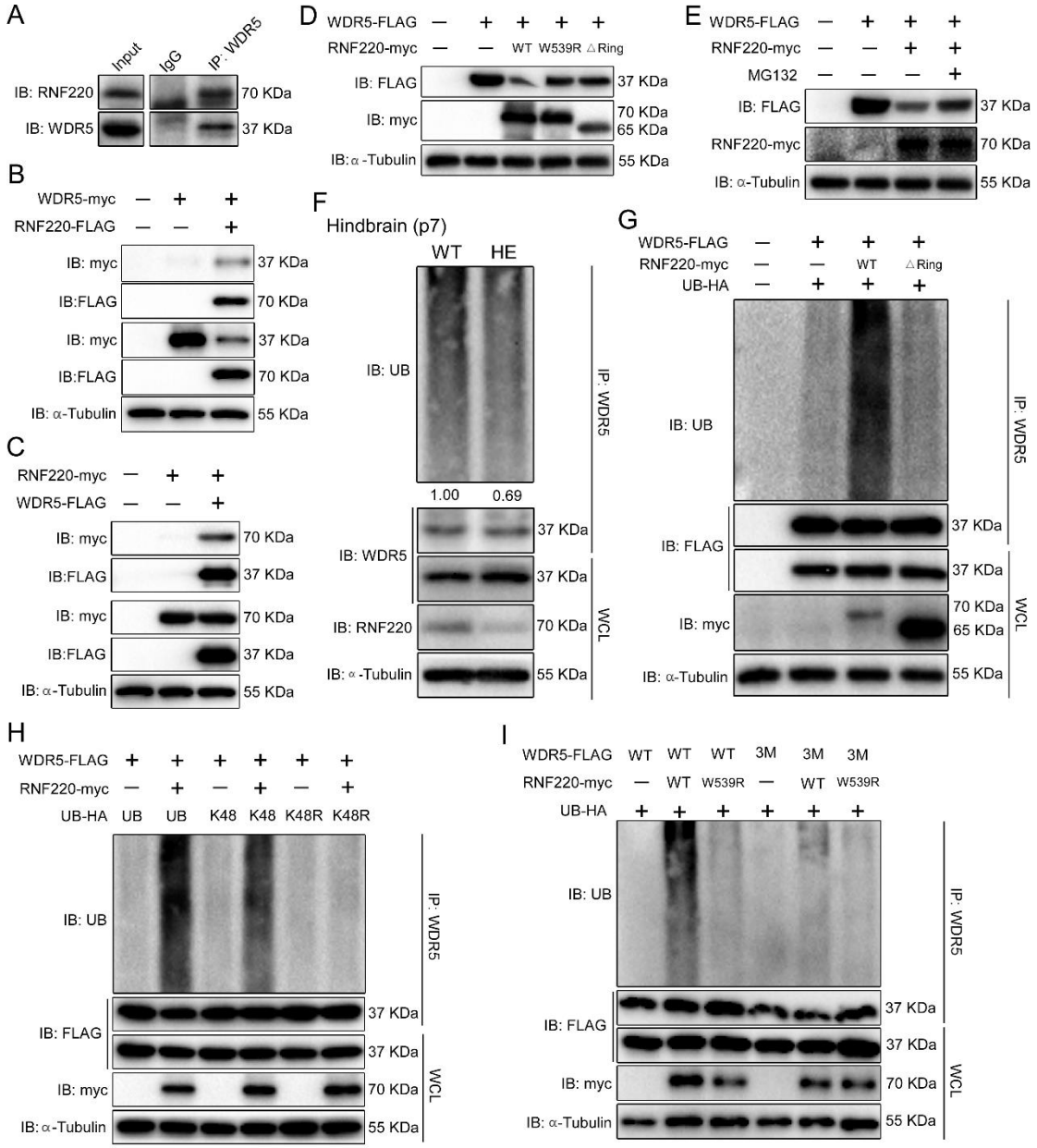

Figure 4. RNF220 interacts with and targets WDR5 for K48-linked polyubiquitination. (**A**) Endogenous co-immunoprecipitation analysis showing the interaction between RNF220 and WDR5 in hindbrains of WT mice. (**B-C**) Co-immunoprecipitation (co-IP) analysis of interactions between RNF220 and WDR5 in HEK293 cells. HEK293 cells were transfected with indicated plasmids and harvested after 48 h. Cell lysates were immunoprecipitated with anti-FLAG beads. Whole-cell lysate and immunoprecipitates were subjected to western blot analysis using indicated antibodies. (**D**) Western blots analysis shows the protein level of

WDR5 when co-expressed with wild type or mutated RNF220 in HEK293 cells. (**E**) Western blots analysis shows the protein level of WDR5 when co-expressed with RNF220 in HEK293 cells in the presence of MG132 or not. MG132 treatment reversed the RNF220-induced decrease of WDR5 protein. (**F**) *In vivo* ubiquitination assays showing the ubiquitination status of WDR5 in hindbrains of WT or *Rnf220*$^{+/-}$ mice. (**G**) *In vivo* ubiquitination assays showing the ubiquitination status of WDR5 when co-expressed with WT or mutated RNF220 in HEK293 cells. (**H**) *In vivo* ubiquitination assays showing RNF220-induced polyubiquitination of WDR5 when the indicated ubiquitin mutations were used in HEK293 cells. (**I**) *In vivo* ubiquitination assays showing the ubiquitination status of the indicated WDR5 mutants when co-expressed with WT or ligase dead RNF220 in HEK293 cells. WT, wild-type. HE, heterozygote. KO, knockout. IB, immunoblot. UB, ubiquitin. WCL, whole cell lysate. △Ring, RNF220 Ring domain deletion. W539R, RNF220 ligase dead mutation. K48, ubiquitin with all lysines except the K48 mutated to arginine. K48R, ubiquitin with the K48 was substituted by an arginine. 3M, substitution of lysines at the positions of 109, 112, and 120 in WDR5 with arginines simultaneously.

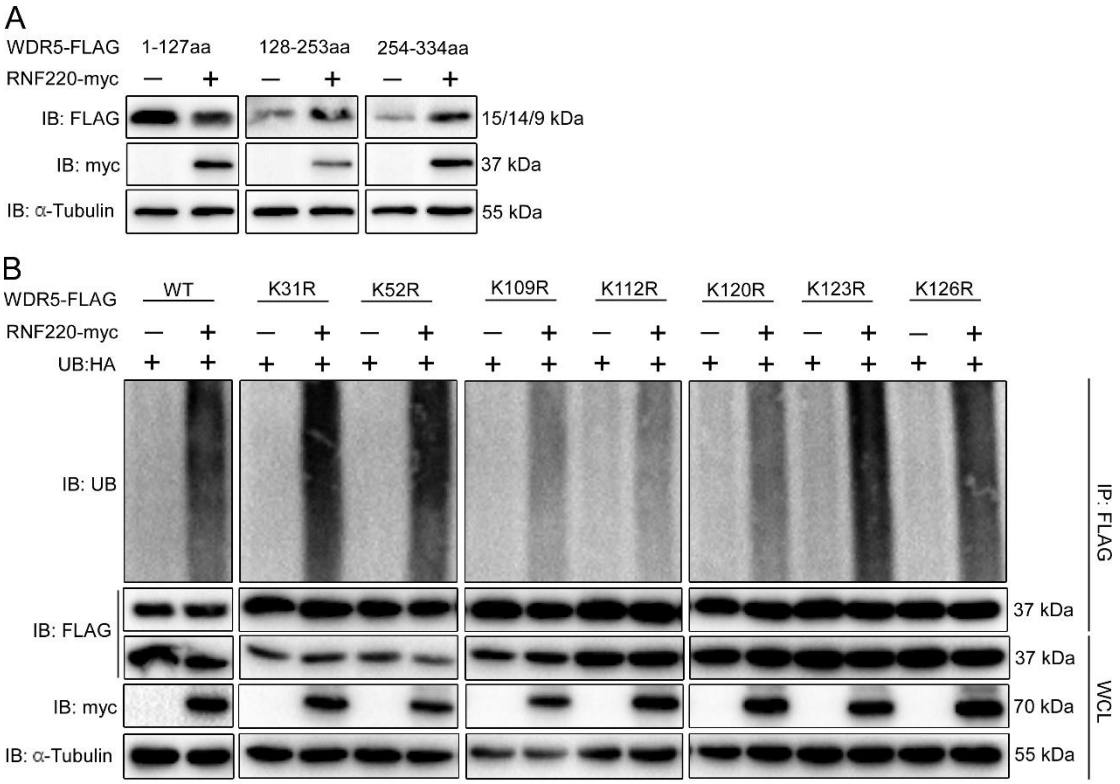

Figure 4-figure supplement 1. RNF220 interacted with and targeted WDR5 for polyubiquitination at multiple lysine sites. (**A**) Western blot analysis of levels of three WDR5 truncated proteins in HEK293 cells when co-transfected with RNF220 or not. (**B**) *In vivo* ubiquitination analysis of ubiquitination status of indicated WDR5 KR mutants when co-expressed with RNF220 or not in HEK293 cells. IB, immunoblot. IP, immunoprecipitation. WCL, whole cell lysate. K31R, K52R, K109R, K112R, K120R, K123R, or K126R, substitution of lysine with arginine in WDR5 at indicated positions.

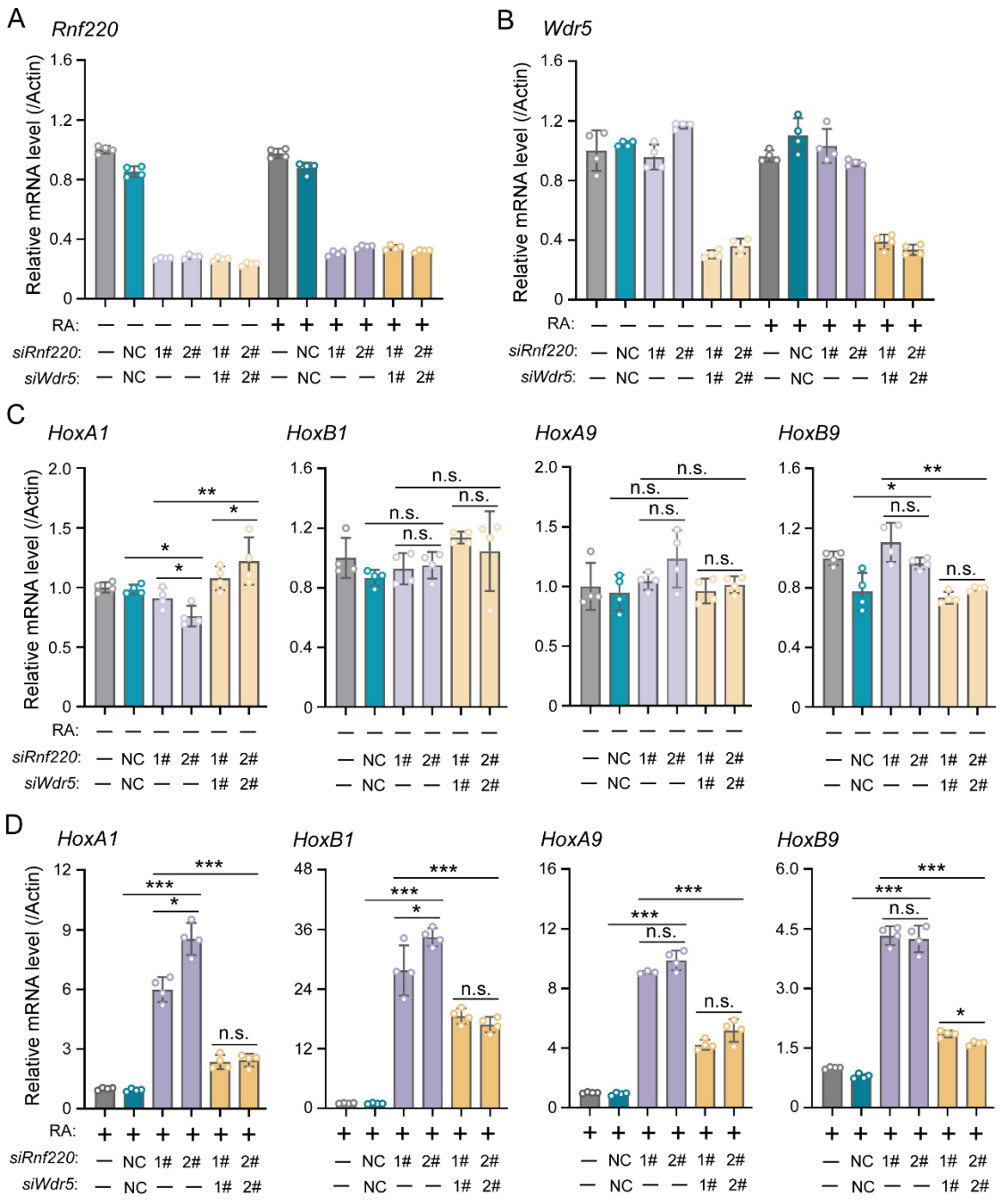

Figure 5. WDR5 recovered *Rnf220* deficiency-induced up-regulation of *Hox* genes in P19 cell line. (**A-B**) qRT-PCR analysis showing the expression levels of *Rnf220* (A) and *Wdr5* (B) when transfected the indicated combinations of siRNAs against *Rnf220* or *Wdr5* in the presence or absence of RA. **(C-D)** qRT-PCR analysis showing the expression levels of *HoxA1*, *HoxB1*, *HoxA9*, *HoxB9* when transfected siRnf220 or both siRnf220 and siWdr5 when treated with RA (D) or not (C). RA: retinoic acid. n.s., not significant. *p< 0.05, **p < 0.01, ***p < 0.001.

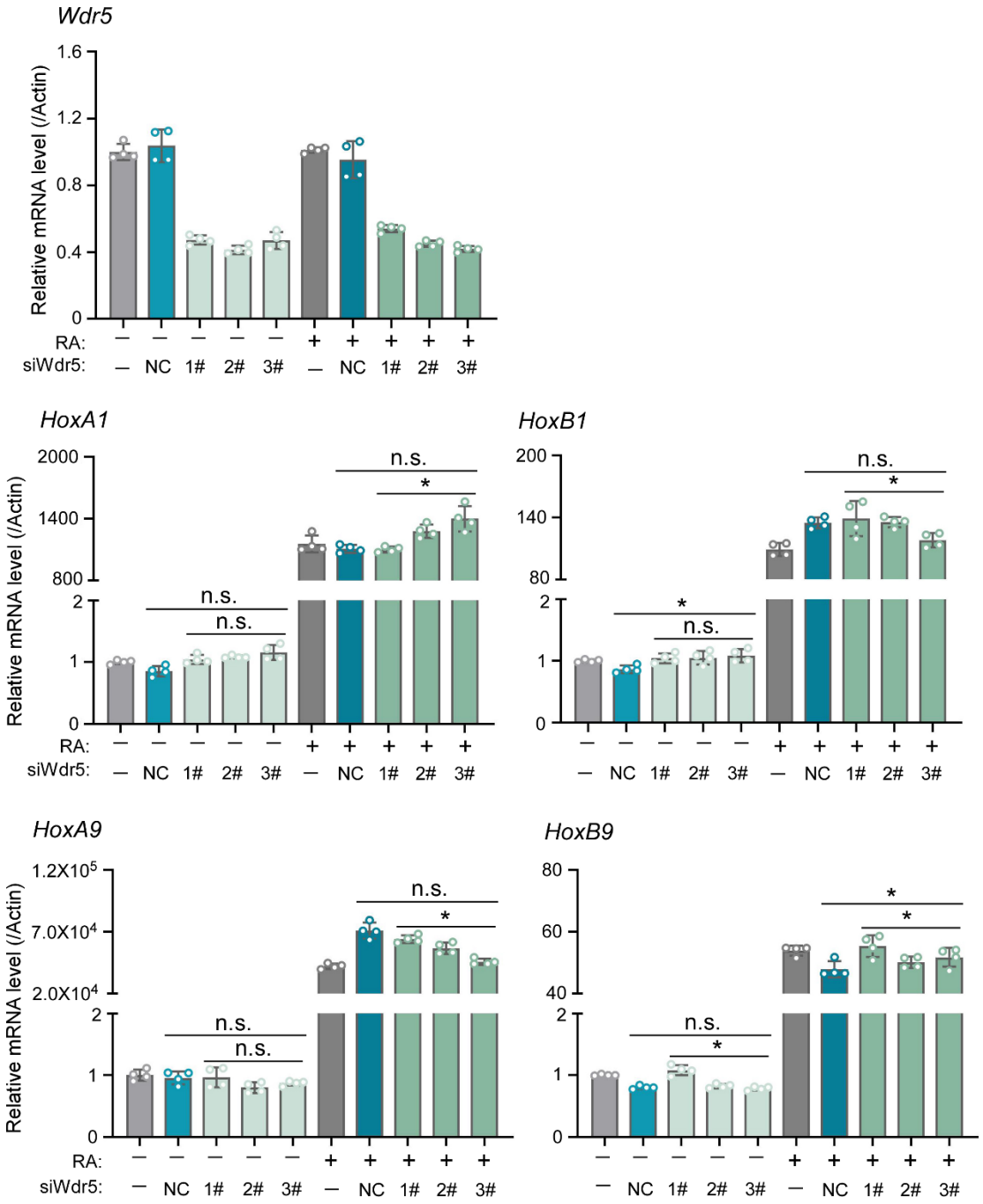

Figure 5-figure supplement 1. WDR5 knockdown had no effect on *Hox* genes in P19 cell line. qRT-PCR analysis of mRNA levels of *WDR5*, *HoxA1*, *HoxB1*, *HoxA9*, and *HoxB9* when WDR5 was knocked down by siRNA transfection in P19 cells with or without RA treatment. RA: retinoic acid. n.s., not significant. *p< 0.05.

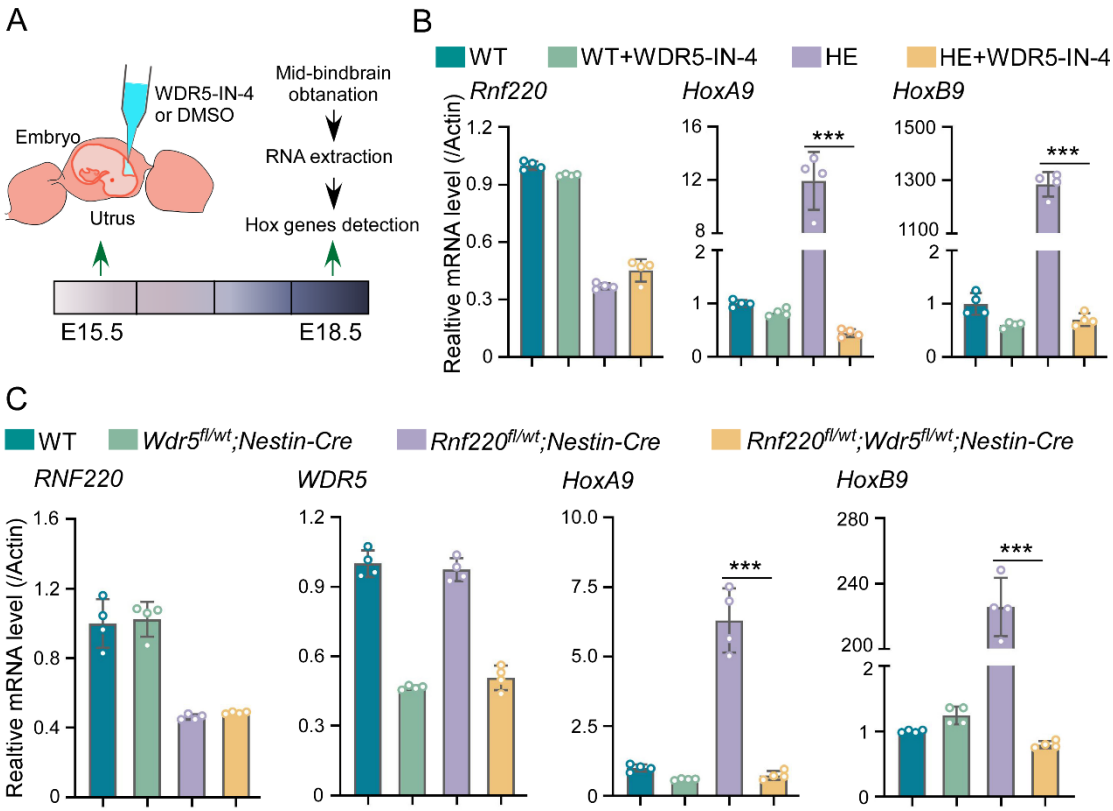

Figure 6. Genetic and pharmacological ablation of WDR5 recovered *Rnf220* deficiency-induced up-regulation of *Hox* genes. (**A**) Diagram of experimental strategy for *in utero* local injection of WDR5 inhibitors. (**B**) qRT-PCR analysis of expression levels of *Rnf220*, *HoxA9*, and *HoxB9* in hindbrains of WT and *Rnf220*$^{+/-}$ mouse embryos treated with WDR5 inhibitors or not at E18.5 (n=3 mice per group). (**C**) qRT-PCR analysis of expression levels of *Rnf220*, *Wdr5*, *HoxA9*, and *HoxB9* in hindbrains of adult mice with indicated genotypes (n=2 mice per group). WT, wild-type. HE, heterozygote. ***$p < 0.001$.

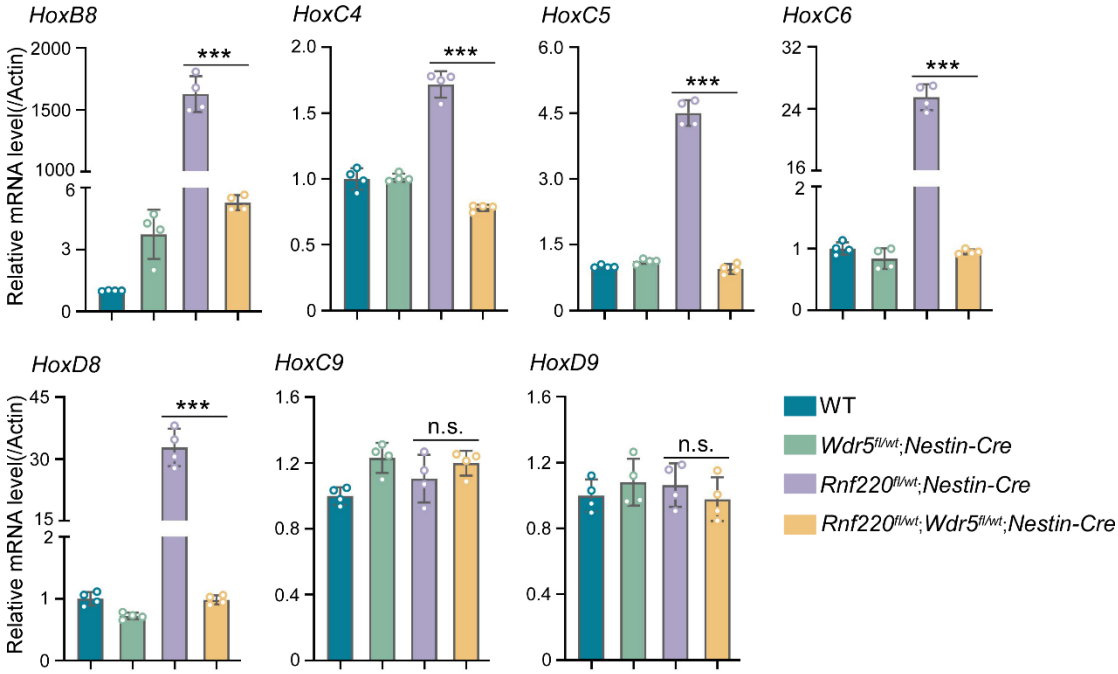

Figure 6-figure supplement 1. Genetic ablation of *Wdr5* reversed *Hox* gene de-repression caused by *Rnf220* deficiency. qRT-PCR analysis of mRNA levels of *HoxB8*, *HoxC4*, *HoxC5*, *HoxC6*, *HoxD8*, *HoxC9*, and *HoxD9* in hindbrains of WT, *Wdr5*$^{fl/wt}$;*Nestin-Cre*; *Rnf220*$^{fl/wt}$;*Nestin-Cre*, and *Rnf220*$^{fl/wt}$;*Wdr5*$^{fl/wt}$;*Nestin-Cre* mice (n=2 mice per group). WT, wild-type. n.s., not significant. ***$p < 0.001$.